Satellite Observations of Onset and Growth of Severe Local Storms

by
Andrew J. Negri

Department of Atmospheric Science
Colorado State University
Fort Collins, Colorado

Principal Investigator: Thomas H. Vonder Haar

Colorado State University

Department of Atmospheric Science

Paper No. 278

SATELLITE OBSERVATIONS OF THE ONSET AND GROWTH OF SEVERE LOCAL STORMS

by

Andrew J. Negri

Department of Atmospheric Science

Colorado State University

Fort Collins, Colorado

December, 1977

Atmospheric Science Paper No. 278

ABSTRACT

On 24 April 1975, numerous severe storms developed in an area extending from southwest Oklahoma to eastern Tennessee during the afternoon and evening hours. Significant severe weather reports included 2.75 in. hail at Wewoka, Oklahoma and a destructive, killer tornado at Neosho, Missouri. An unusually comprehensive data set was available on this day that included: 5-minute interval SMS visible and infrared radiances from 1800 to 0200 GMT; intensity contoured radar reflectivities; special upper-air analyses from NASA's Atmospheric Variability Experiment; and low-level wind fields from satellite inferred cumulus velocities.

The mesoscale nature of the forcing and evolution of these storms is investigated, with emphasis on techniques to aid in the early detection of such severe events. In the pre-storm environment (t-4 to t-2 hours), the satellite wind fields were combined with moisture parameters to derive horizontal moisture flux information. Low level moisture convergence of 1.5×10^{-3} g $kg^{-1} s^{-1}$ or greater was indicative of regions of subsequent severe storm genesis. Dynamic parameters such as boundary layer vorticity production and relative vorticity were also useful prognosticators of subsequent severe activity.

In the first 30 minutes of cloud lifetime, infrared (IR) cloud growth rates of 2×10^{-3} s^{-1} or greater accurately indentified potential severe storms. Little success was realized in forecasting the exact time of the severe event on the ground. A comparison of IR determined cloud tops with radar observed tops illustrated particular problems

in inferring cloud height for storms penetrating the tropopause. The need for rapid-time interval satellite coverage is stressed, as is the need for a computer-linked video system to process and interpret data.

TABLE OF CONTENTS

LIST OF TABLES

LIST OF FIGURES

1.0 INTRODUCTION

With the launch of geostationary satellites in the late 1960's, a new era was introduced in the prediction, detection, and understanding of the atmospheric phenomena known as severe local storms. A sequence of satellite images provides one with an immediate feel for the dynamics of the situation one is observing. The combination of satellite measurements with conventional surface and upper air observations provides a more complete description of "weather" than either method alone.

It is the purpose of this study to use such a combination of data sources in the development of techniques to better predict the occurrence and severity of severe local storms. A working definition of the phenomena is first needed:

Severe Local Storms (SELS): dangerous storms that usually cover relatively small geographic areas or move in narrow paths and are of a sufficient intensity to threaten life and property.*

For the purposes of this study, severe events included tornadoes, funnel clouds, and thunderstorms with either hailstones greater than 0.75", or wind gusts greater than 50 knots. The aim of the prediction scheme to be described is to provide a "point" forecast one to two hours prior to the onset of a severe storm. The technique requires high temporal frequency satellite data (5-15 minutes) and a computer-linked video system that allows for man-machine interaction. Both were available in this "after-the-fact" diagnostic study.

---

*National Severe Local Storms Operations Plan, U.S. Department of Commerce--NOAA, Washington, D.C., 1977, 38 p.

The day chosen for study was 24 April 1975, when several severe storms developed across an area from southwestern Oklahoma to eastern Tennessee during the afternoon and evening hours. Significant reports included 2.75" hail near Wewoka, Oklahoma and a destructive tornado at Neosho, Missouri. As will be demonstrated in later sections, the outbreak of these large convective storms was due in large part to mesoscale (meso-β), not synoptic scale forcing. The infamous "super-outbreak" of tornadoes on 3-4 April 1974 is a classic example of a large mesoscale (meso-α) development controlling the outbreak of these storms. Among the recommendations of a panel on severe storms formed soon after this outbreak were:

1) better detection and tracking of convective activity
2) development of better statistical relationships between convective storms and the large mesoscale disturbances that produce them
3) improvement in the dynamical prediction of these large mesoscale disturbances*

The first and third recommendations are addressed directly in this study.

The monitoring of the pre-storm environment is of utmost importance in determining areas of subsequent severe weather. One type of monitoring can be accomplished through the use of low-level wind fields derived from satellite determined cumulus velocities. These fields can provide horizontal moisture flux information when coupled with an appropriate moisture parameter (mixing ratios, precipitable

*Severe Storms-Prediction, Detection and Warning, National Academy of Sciences, Washington, D.C., 1977, 78 p.

water). Storms must necessarily grow in areas of moisture convergence, and one attempt of this study will be to compare the magnitude of such convergence with subsequent storm severity. The dynamic parameters of boundary layer vorticity production and relative vorticity will also be investigated with respect to severe storm activity. Table 1-1 is a comprehensive list of objective indicators of severe storm activity.

Continued remote sensing of the cloud field in its growth phase is then accomplished through the use of satellite infrared radiances. Rates of growth for several storms of differing severity are examined in an attempt to develop criteria for a short-term prediction-warning scheme. The problem becomes challenging because direct identification of tornadoes or regions of heavy precipitation is not possible when viewing the storm from above; the internal structure of the storm is hidden from both optical and infrared sensors. Fujita (1973) has shown that the height of cloud-tops can undergo fluctuations indicative of the changes in the intensity of updrafts within the storm. It is this type of indirect approach that will be undertaken here.

A final section on the comparison of satellite and radar data for severe storms will detail some particular problems in infrared remote sensing of cloud dynamics. Limitations in the detection of small, intense echo areas and overshooting domes are discussed, as is the investigation of radar and satellite determined cloud heights for storms penetrating the tropopause.

Table 1-1. Objective Indicators of Severe Storm Activity (from Endlich and Mancuso, 1968)

Quantity	Rating	Remarks
High wind speed in low levels. . .	Poor. .	These conditions are generally present in severe storm areas, but also cover extensive regions without severe storms. Thus, they appear inferior to other quantities as indicators.
High temperature and humidity in low levels	Poor. .	
Large moisture gradient near 700 mb.	Poor. .	
High wind speed in upper troposphere	Poor. .	
Large temperature gradient at tropopause level.	Poor. .	
Unstable lapse rate between low and midtroposphere.	Fair. .	The most unstable lapse rate and most unstable index lie generally south of severe storm areas.
Unstable Showalter index	Fair. .	
Area between low-level temperature and moisture axes	Fair. .	These axes are not always well developed.
Destabilizing temperature and advection between low and mid-troposphere	Good. .	
Proximity to 4260 m - thickness line (850-500 mb) and to thickness ridge.	Good. .	
Area of negative vorticity of wind shear vector between low and midtroposphere.	Good. .	
Horizontal divergence in upper troposphere	Good. .	
Upward vertical motion at top of boundary layer.	Good. .	
Negative values of $\nabla \cdot MV$ and of $\nabla \cdot TV$ in low levels	Good. .	*
Vorticity production in low levels.	Good. .	*
Frontogenesis of temperature and of moisture in low levels	Good. .	
Destabilizing distribution of $\nabla \cdot TV$ between low and mid-troposphere	Good. .	

*Examined in this study

2.0 CASE STUDY: 24 April 1975

2.1 Synoptic Situation

On 24 April 1975, numerous severe storms occurred in a region stretching from southwest Oklahoma to eastern Tennessee during the afternoon and evening hours. Figure 2-1 is the surface analysis at 1600 GMT (1000 LST). A cold frontal boundary in the Oklahoma Panhandle extended northeastward through Kansas and Missouri, where it became stationary. An intense moisture gradient existed across a dry line in western Oklahoma. Extremely dry air (dew points 28°-48°F) was moving slowly westward from the Texas plains. Horizontal wind shear across this dry line enhanced the convergence of moist air (dew points 63°-70°F) in eastern Texas and Oklahoma. A dissipating squall line from the previous day's convective activity separated hot, moist air in the warm sector from cooler air produced by nocturnal thunderstorm activity.

The evolution of the surface system is portrayed in Figure 2-2, the surface analysis five hours later at 2100 GMT. The western portion of the cold front had moved a considerable distance southward under the influence of 20-25 kt northerly winds. Light winds in the air mass behind the dry line caused only a slight eastward shift of that boundary. South of the front, a narrow tongue of hot, dry air had advanced northeastward into a low pressure area forming on the Oklahoma-Kansas border. This type of sub-synoptic scale low, shown in Figure 2-2, frequently occurs with tornado-producing storms (Tegtmeier, 1974), and this case was no exception. The nocturnal thunderstorm boundary is still evident in the temperature field and is shown as a dissipating warm front. Boundaries of this type have been shown to be important in severe storm

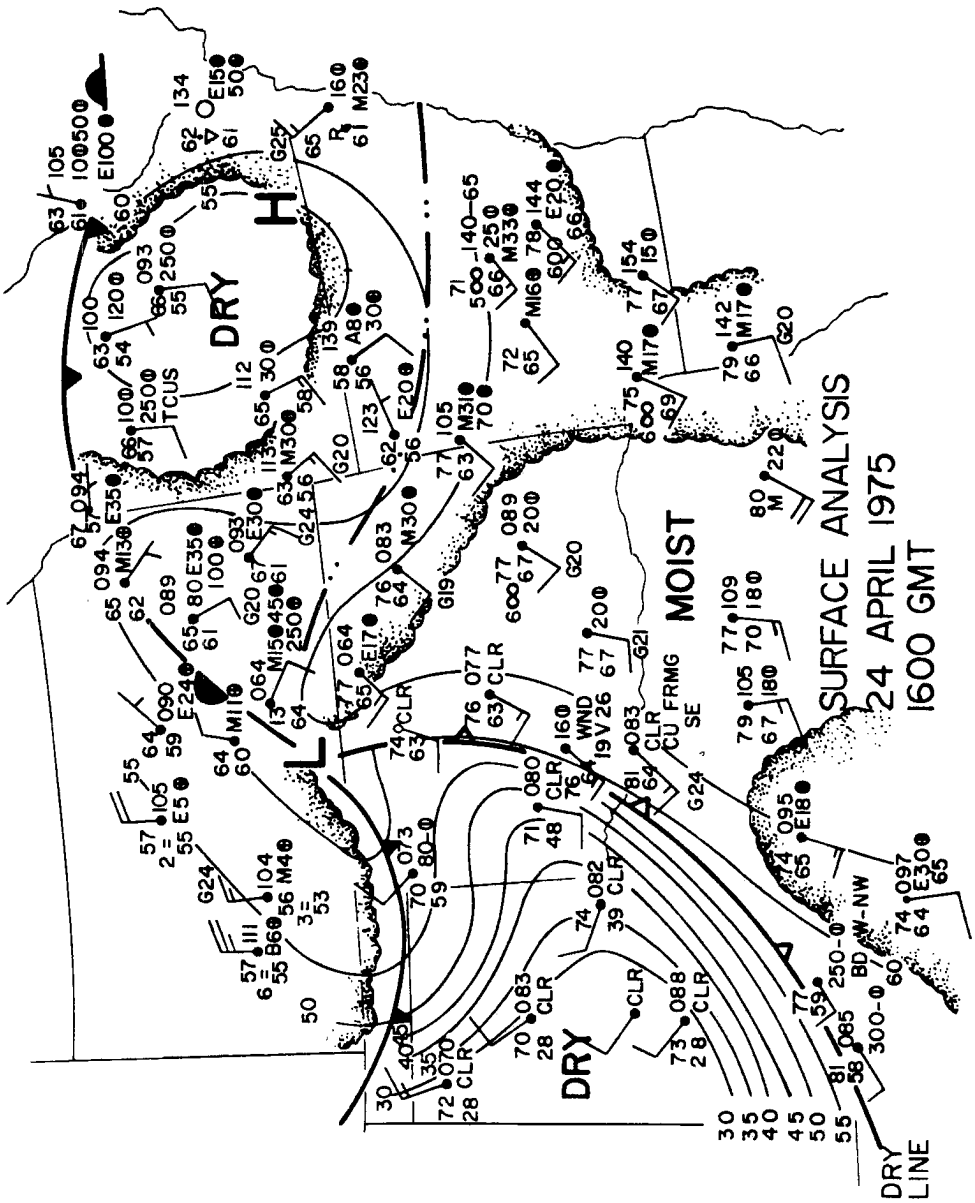

Figure 2-1 Surface analysis 24 April 1975 1600 GMT.

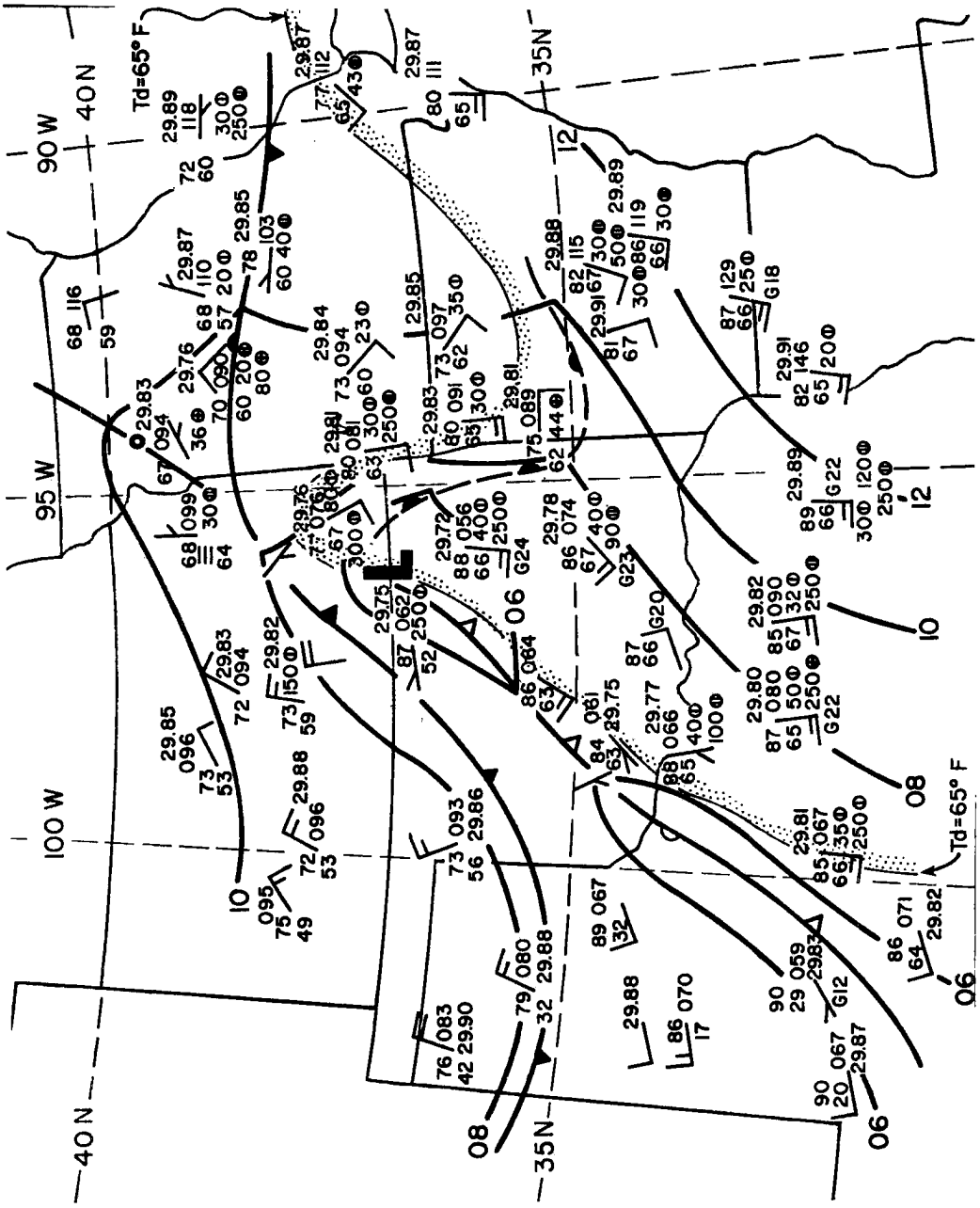

Figure 2-2 Surface analysis 24 April 1975 2100 GMT.

genesis when they intersect frontal boundaries (Purdom, 1976a). In the warm sector, temperatures had climbed into the upper 80's with dew point temperatures in the high 60's.

A comprehensive set of upper air data was available every three hours this day from NASA's fourth Atmospheric Variability Experiment (AVE IV). The 500 mb analysis at 2100 GMT (Figure 2-3) showed a weak shortwave trough extending south from Kansas into central Texas. The upper air flow field split into two regimes west of the Rocky Mountains. A stronger shortwave, within the northern stream, finally merged with the southern wave by 0000 GMT on the 25th. Although severe storm activity occurred throughout the night, the most intense storms were those associated with the southernmost wave during the period 2300-0200 GMT on the 24th through 25th.

The 300 millibar analysis at 2100 GMT is portrayed in Figure 2-4. A shortwave trough centered in South Dakota and Nebraska was advancing southeastward into a region of upper level difluence. This difluent region was located between a polar jet stream of 70-80 knot winds and a subtropical jet of 60-70 knot winds. Whitney (1977) has found that this type of difluent configuration ahead of an advancing trough is favorable for severe storm development. Whitney found that in the April 24 case, as in other cases, the greatest potential for release of conditional instability existed north of the subtropical jet.

The Skew T/Log P plot of the upper air sounding taken at Monett, Missouri (UMN) at 2100 GMT is shown in Figure 2-5. The sounding is typical of a classic severe storm sounding, with a low level moisture source capped by an inversion and dry air aloft. In the boundary layer, mixing ratios were almost 12 g kg^{-1}, and veering winds indicated low

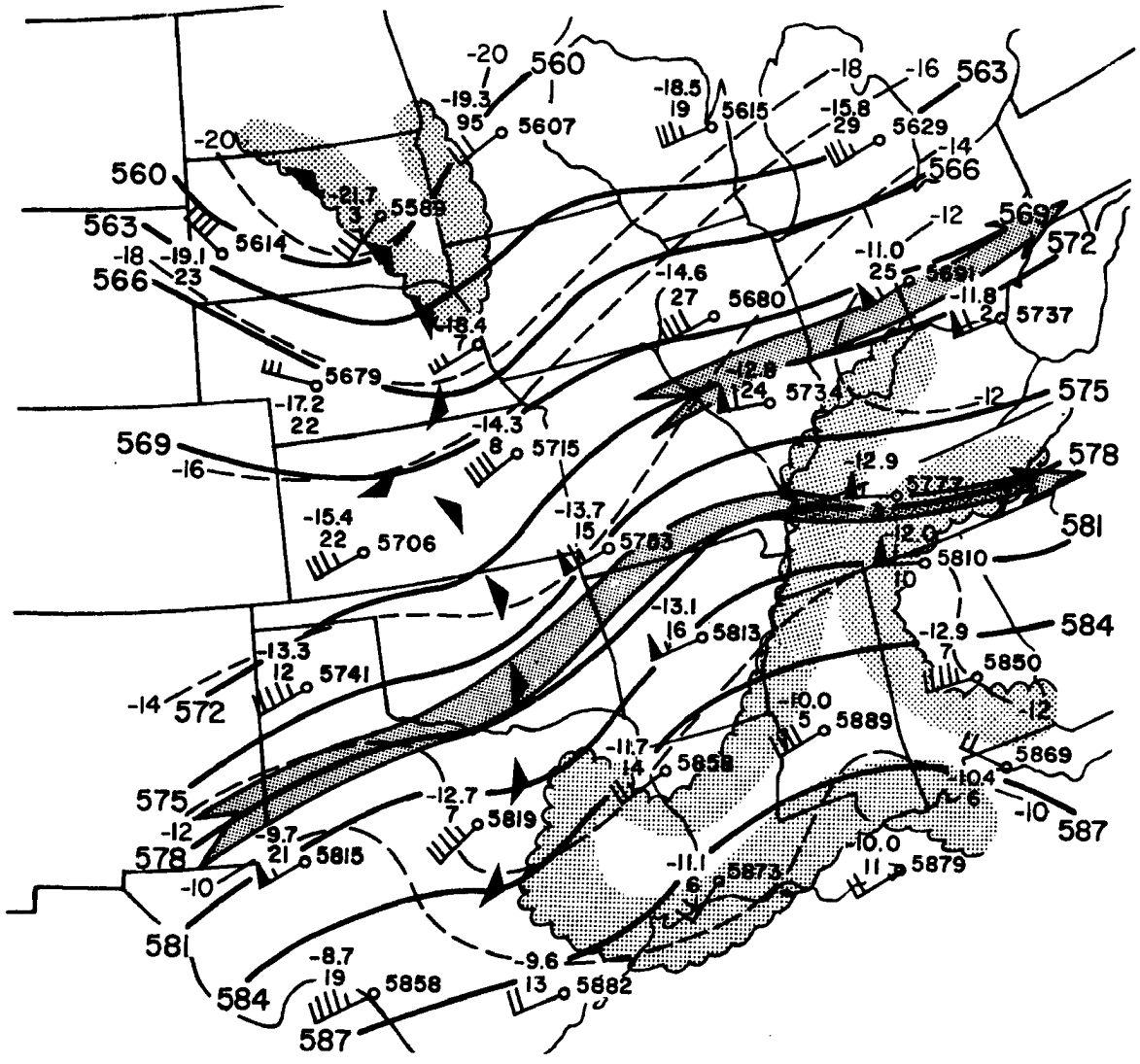

Figure 2-3 500 millibar analysis 24 April 1975 2100 GMT.

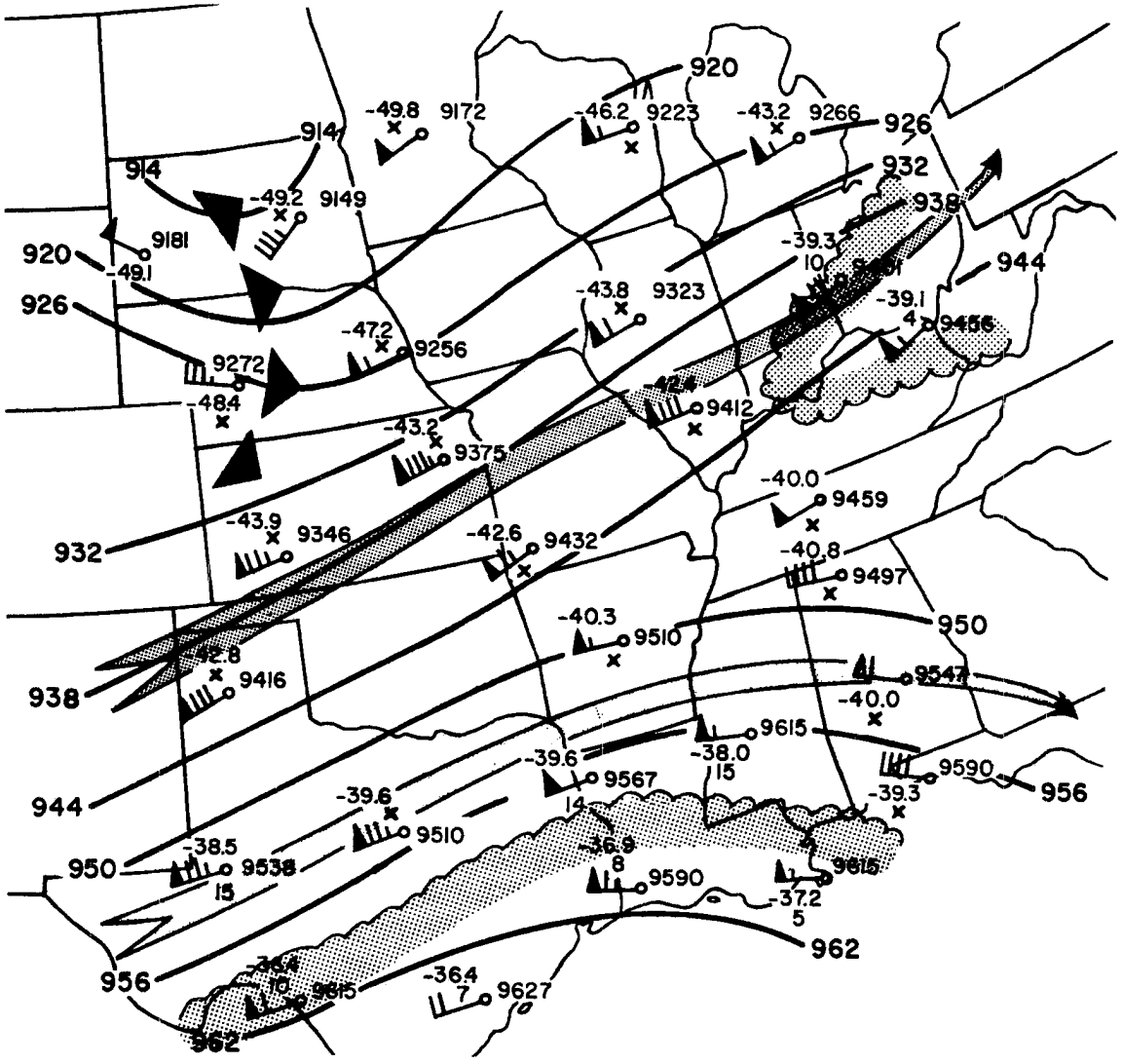

Figure 2-4 300 millibar analysis 24 April 1975 2100 GMT.

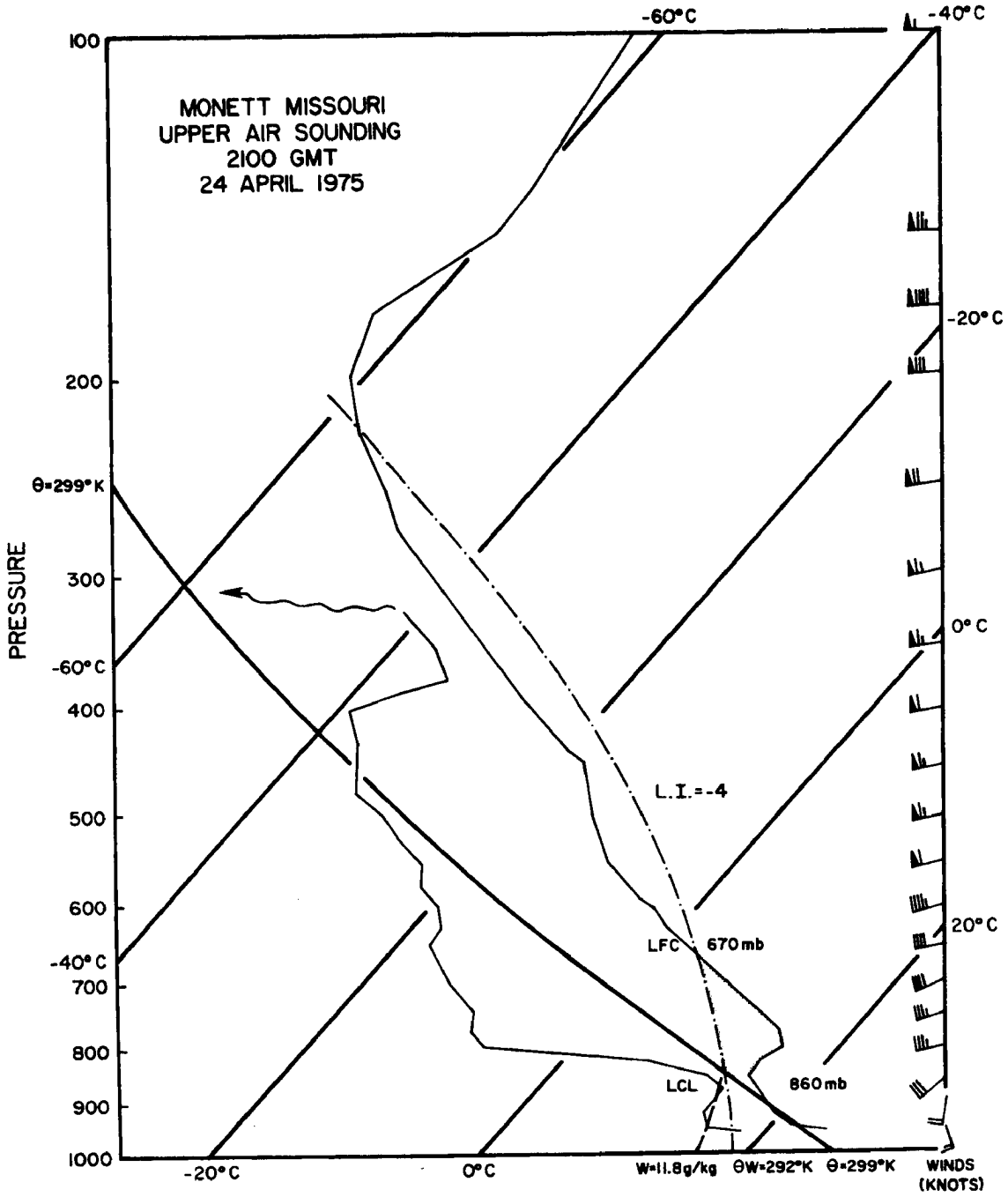

Figure 2-5 Monett, Missouri upper air sounding 24 April 1975 2100 GMT.

level warm air advection. The sounding's lifted index (LI) was -4, indicative of the substantial buoyancy a subcloud parcel of air would have if lifted to 500 mb. A large area of negative buoyancy is also apparent in the 200 mb layer between the lifted condensation level (LCL) and the level of free convection (LFC).

Using the AVE IV sounding data, Wilson (1976) computed the synoptic scale vertical motion field (ω) using a kinematic method. His 700 mb ω field at 2100 GMT is shown in Figure 2-6, with units of μbars/sec. Regions where severe storms developed are cross-hatched. The large-scale vertical motion fields apparently did not organize the convection on this day; storms developed in regions of diagnosed subsidence or of only slight upward motion. The mesoscale nature of the dominate forcing mechanisms is discussed in subsequent chapters.

2.2 Severe Storm Reports

Due to a combination of synoptic scale features (cold front, advancing upper level trough, upper level difluence) and mesoscale organization (subsynoptic low, dry line) several severe storms developed in the afternoon and evening hours of 24-25 April. Reports from Storm Data* have been summarized in Figure 2-7. The operational range of radar sites at Little Rock (LIT), Oklahoma City (OKC), and Kansas City (MKC), are also shown. Radar data from crucially located Monett, Missouri were not recorded. Significant storm reports included: hailstones of 2.75 in. (7.0 cm) diameter at Wewoka, Okhaloma at 2315; a tornado near Blue Jacket, Oklahoma at 0000 GMT; and a tornado at Neosho, Missouri at 0040. This later tornado caused three deaths, 22 injuries and $10.5 million in property damage.

*A monthly publication of the Environmental Data Service of the National Oceanographic and Atmospheric Administration.

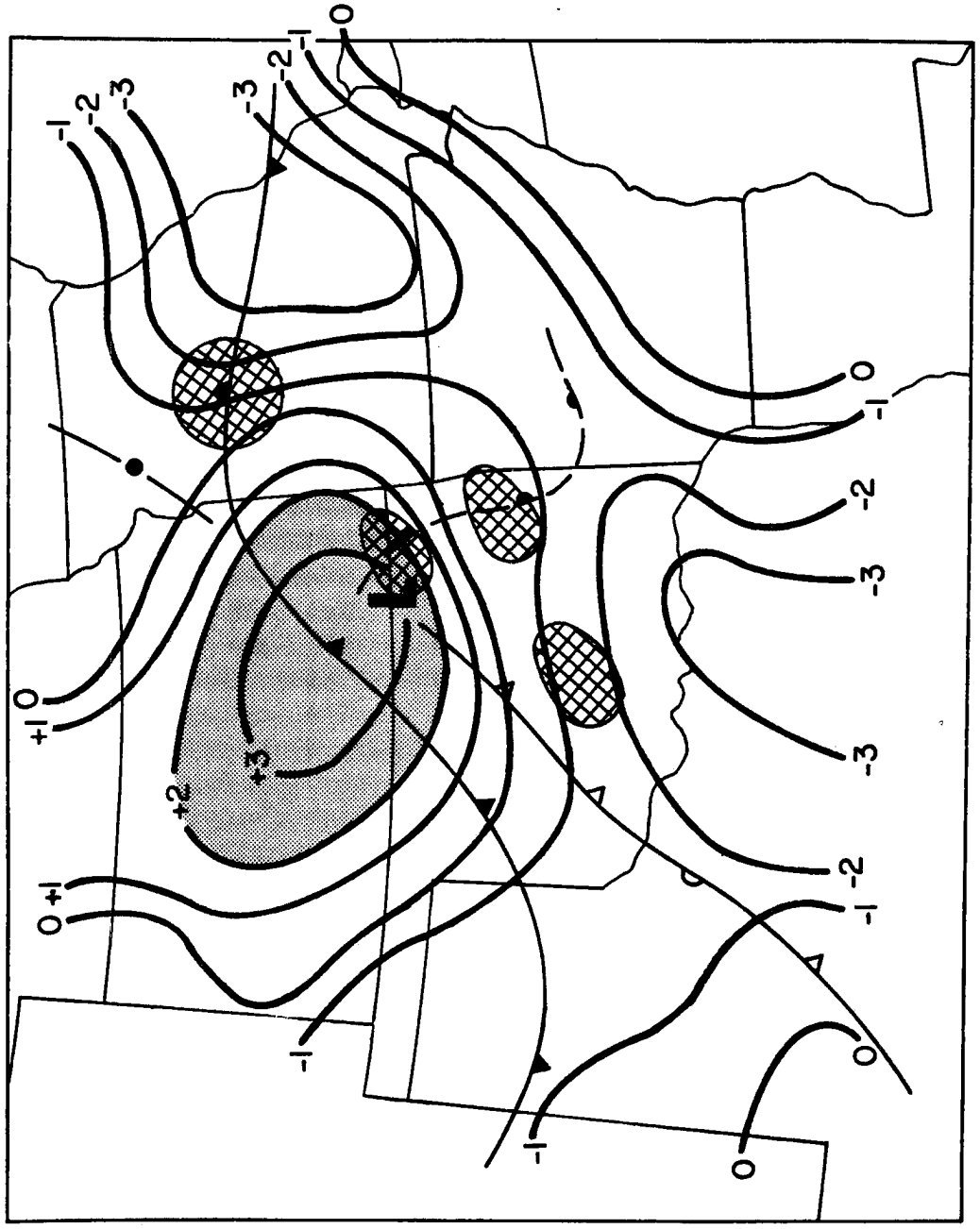

Figure 2-6 700 millibar vertical velocity in μbars s^{-1} (from Wilson, 1976). Regions where severe thunderstorms developed are cross-hatched.

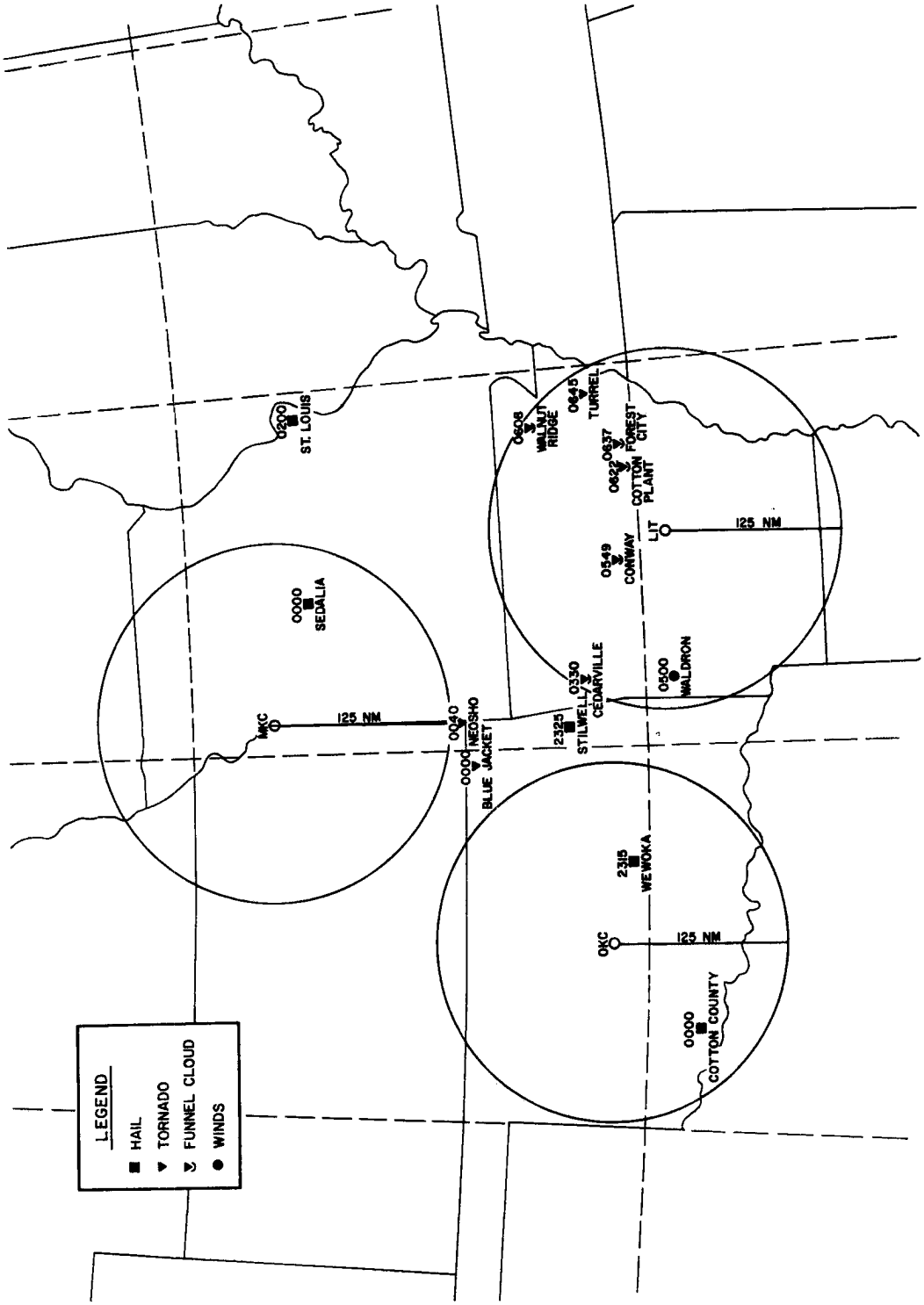

Figure 2-7 Severe storm reports 24-25 April 1975.

3.0 MESOSCALE WINDS AND MOISTURE

3.1 A Wind Tracking System - AOIPS

Five minute interval SMS visible channel data of 1 km resolution were used to derive low-level wind fields by tracking small cumulus clouds. Winds were tracked on NASA's Atmospheric and Oceanographic Information Processing System (AOIPS)*. A complete description of the AOIPS and cloud tracking techniques is given by Billingsley (1976). The day chosen as a case study was 24 April 1975, in an area approximately 10 degrees on a side centered near Oklahoma City, Oklahoma. Intense convective development occurred 2-3 hours after the tracking time. A time series of rapid time interval (5 minute) SMS digital data was selected; for example, a sequence comprised of the 2057-2102-2107-2112 GMT images (see Figure 3-1). These images were navigated (by a landmark registration technique), processed into a television loop, and displayed on a Hazeltine image processor (Figure 3-2). A specific cloud element was then selected and an electronic cursor was used to specify the cloud's location throughout the loop. The cursor was positioned near the rear of the cloud (relative to its movement) to avoid propagation and shear contamination of the velocity field. The velocity of the cloud element is computed from its location on successive images, knowing the time interval between images.

The acceptance of a wind vector into the data set was based on two considerations:

*Colorado State University has an equally sophisticated system, the All Digital Video Imaging System for Atmospheric Research (ADVISAR). See Appendix A.

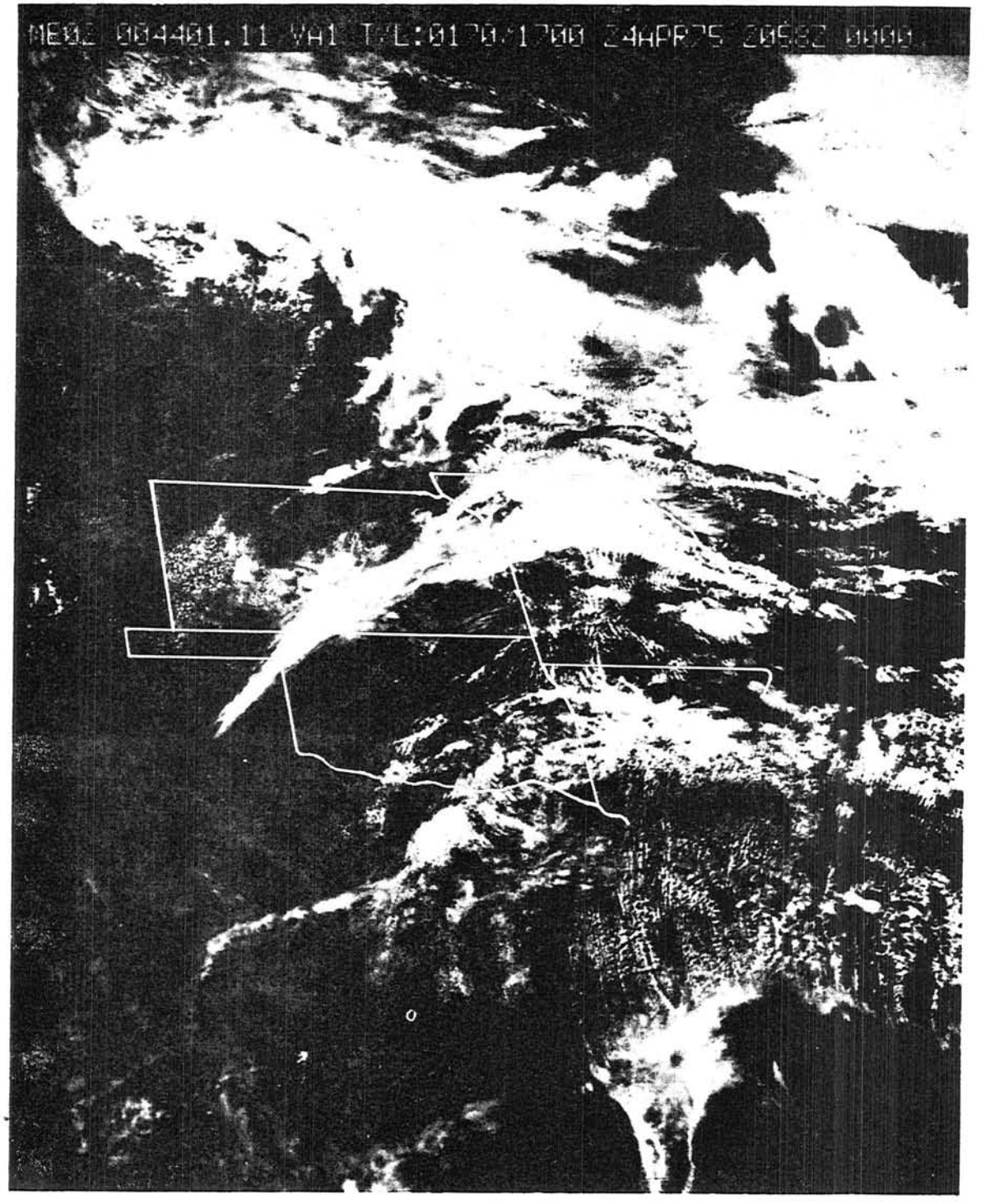

Figure 3-1 SMS-2 visible channel image at 2058 GMT.

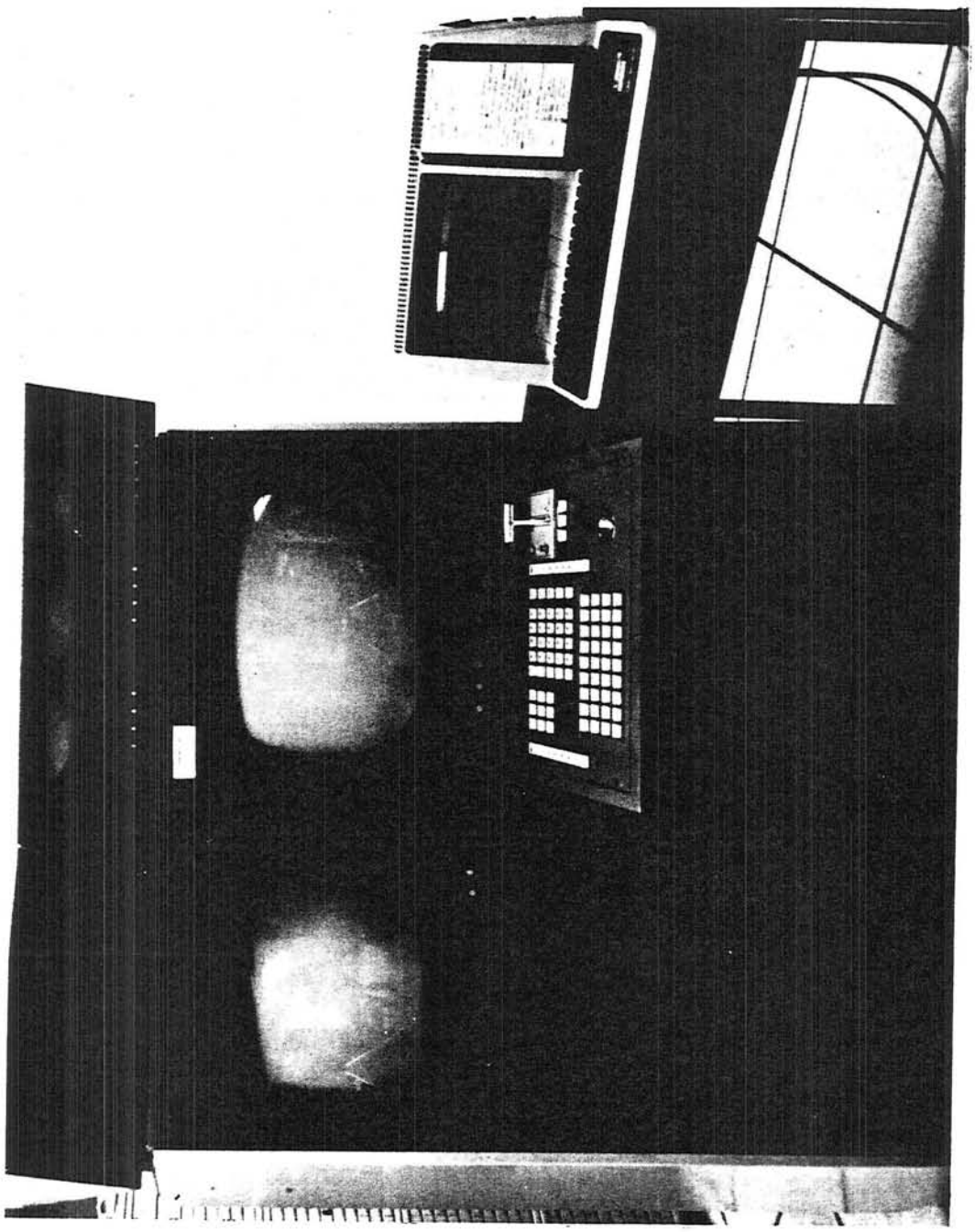

Figure 3-2 A portion of the AOIPS used for cloud tracking.

1. On an objective basis, the statistics on cloud motion (Table 3-1) are examined for consistency and representativeness, e.g., a cloud element should not be accelerating greatly.

2. On a more subjective basis, the vector is shown superimposed on the loop, again in an attempt to determine its representativeness of the cloud motion.

A "complete" data set consisted of 100-300 vectors.

3.2 Satellite Derived Wind Fields

Two complete wind sets tracked on the AOIPS are shown graphically in Figure 3-3 (1800 GMT) and Figure 3-4 (2100 GMT). Lengths are scaled such that a vector of length one degree represents a wind speed of 17.8 ms^{-1} u velocity and 22.2 ms^{-1} v velocity. Voids exist in the data where either high cirrus clouds or mid-level altocumulus obscured the low-level cumuli, or in the dry stable air where convection was inhibited. In Figure 3-4, the frontal region running E-W through Kansas and Missouri is an example of the former (obscuration of low clouds) while the area behind the dry line in north central Oklahoma illustrates the latter (refer to surface analysis, Figure 2-1).

Results of previous studies have indicated that cumulus motion represents mean winds in the subcloud layer to within 5 degrees and 1 ms^{-1} (Fujita et al., 1975 and Hasler et al., 1975). More recently, Suchman and Martin (1976) explored the accuracy and representativeness of tracer winds in the GATE* area. They found that ship winds used as "ground" truth differed from satellite winds by less than 3 ms^{-1}. Using 30-minute interval imagery (as compared to 5 minute in this study), they

*Global Atmospheric Research Program Atlantic Tropical Experiment

Table 3-1 Statistics on Cloud Location and Motion

Cloud #	Vector ID	u (ms^{-1})	v (ms^{-1})	Speed (ms^{-1})	Direction (degrees)		Latitude (°N)	Longitude (°W)
23	1-2	12.77	12.62	17.95	225.33	IMAGE1	35.0503	96.2058
	2-3	11.92	9.29	15.11	232.08	IMAGE2	35.0841	96.1640
	1-3	12.34	10.95	16.50	228.42	IMAGE3	35.1090	96.1250
	3-4	14.80	9.77	17.73	236.57	IMAGE4	35.1351	96.0767
	2-4	13.36	9.53	16.41	234.50			
	1-4	13.16	10.56	16.87	231.26			

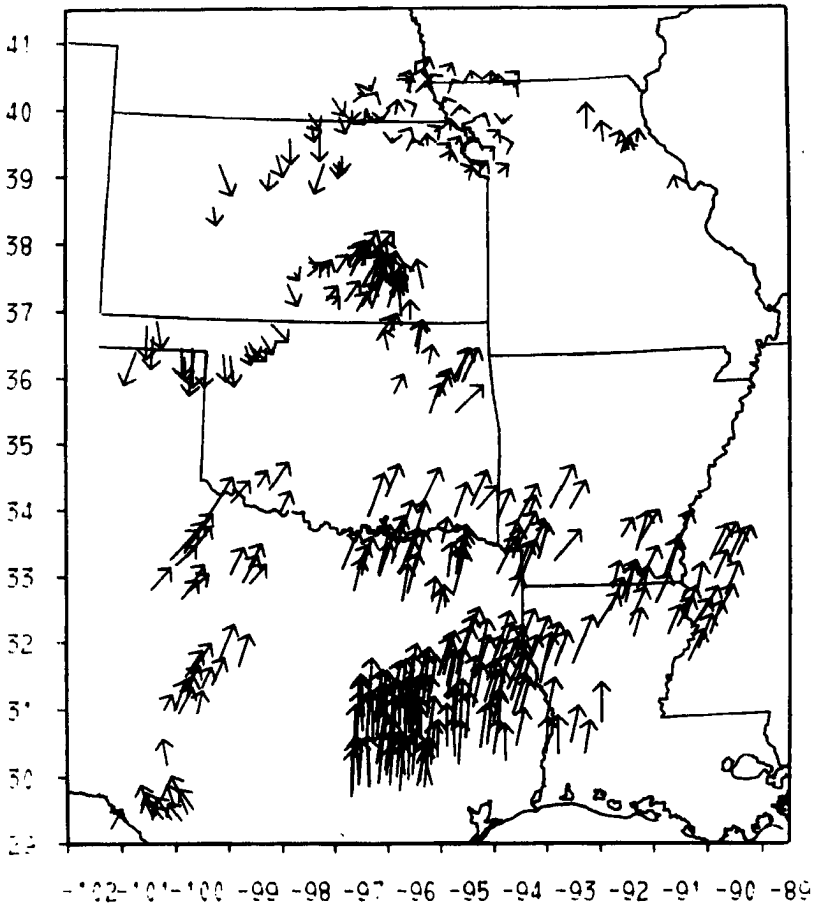

Figure 3-3 Satellite derived wind field at 1800 GMT.

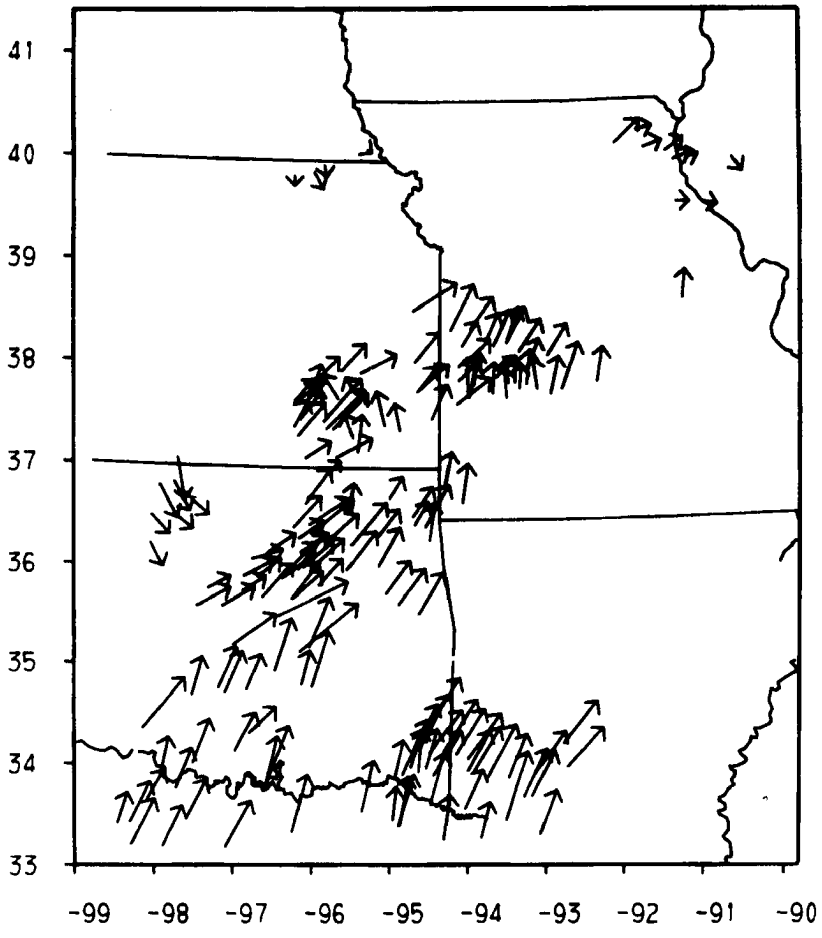

Figure 3-4 Satellite derived wind field at 2100 GMT.

found a reproducibility of 1.3 ms^{-1} for cumulus level winds. Cumulus tracked winds would seem to better indicate boundary layer motion than do corresponding surface winds because:

1. a 20-minute "average" of mean flow is obtained,

2. surface winds are influenced by topography and surface stress.

Doswell (1976) recognized the importance of using "filtered" surface data in computations of low-level moisture divergence.

The wind fields of Figures 3-3 and 3-4 were then objectively analyzed by the cubic spline technique. This procedure was initially used by Fritsch (1971) in analyses of two-dimensional fields. The objectively analyzed fields at 1800 and 2100 GMT are shown in Figures 3-5 and 3-6 respectively, with the vectors scaled as in Figure 3-3. For the 1800 GMT field, the grid interval is 0.5 degrees, while for the 2100 GMT field it is 0.4 degrees. This was done to minimize computer calculations in the 1800 field, due to its larger area and higher density of wind vectors. For the 2100 wind field, the spatial distribution of the data indicate that the validity of the gridded winds would be most questionable over the northwestern and southeastern corners of the domain; however, these regions were not affected by storms.

3.3 Moisture Convergence

Several researchers, including Hudson (1971) and Sasaki (1973) computed surface moisture convergence and found good agreement between those patterns and reports of severe weather several hours later (see Figure 3-7a and b). Intense moisture convergence ($\sim 10^{-3}$ g kg^{-1} s^{-1}) is one condition found favorable for tornadic storm development (Sasaki, 1975). Previous work by this author and others (Negri et al., 1971

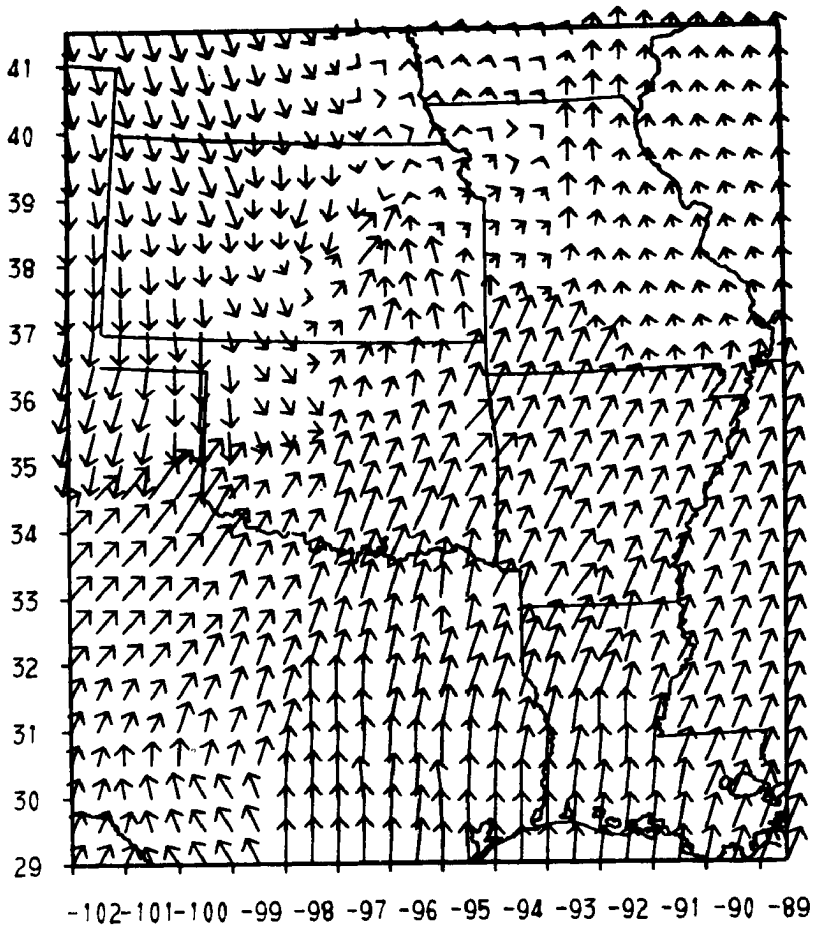

Figure 3-5 Objectively analyzed wind field at 1800 GMT.

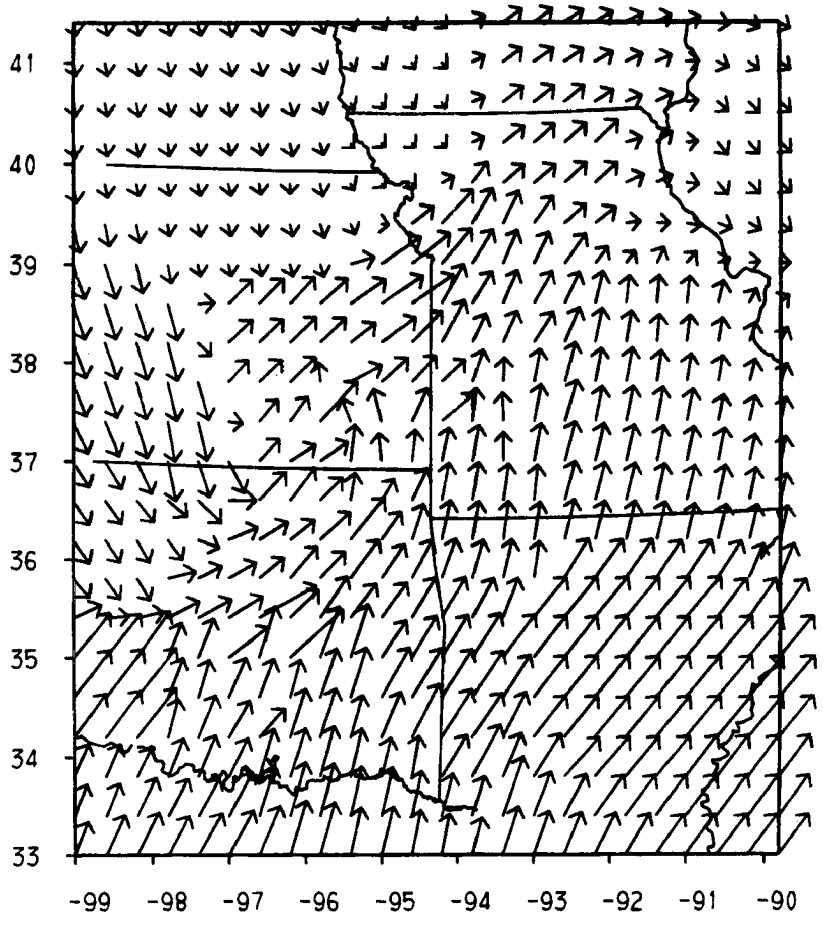

Figure 3-6 Objectively analyzed wind field at 2100 GMT.

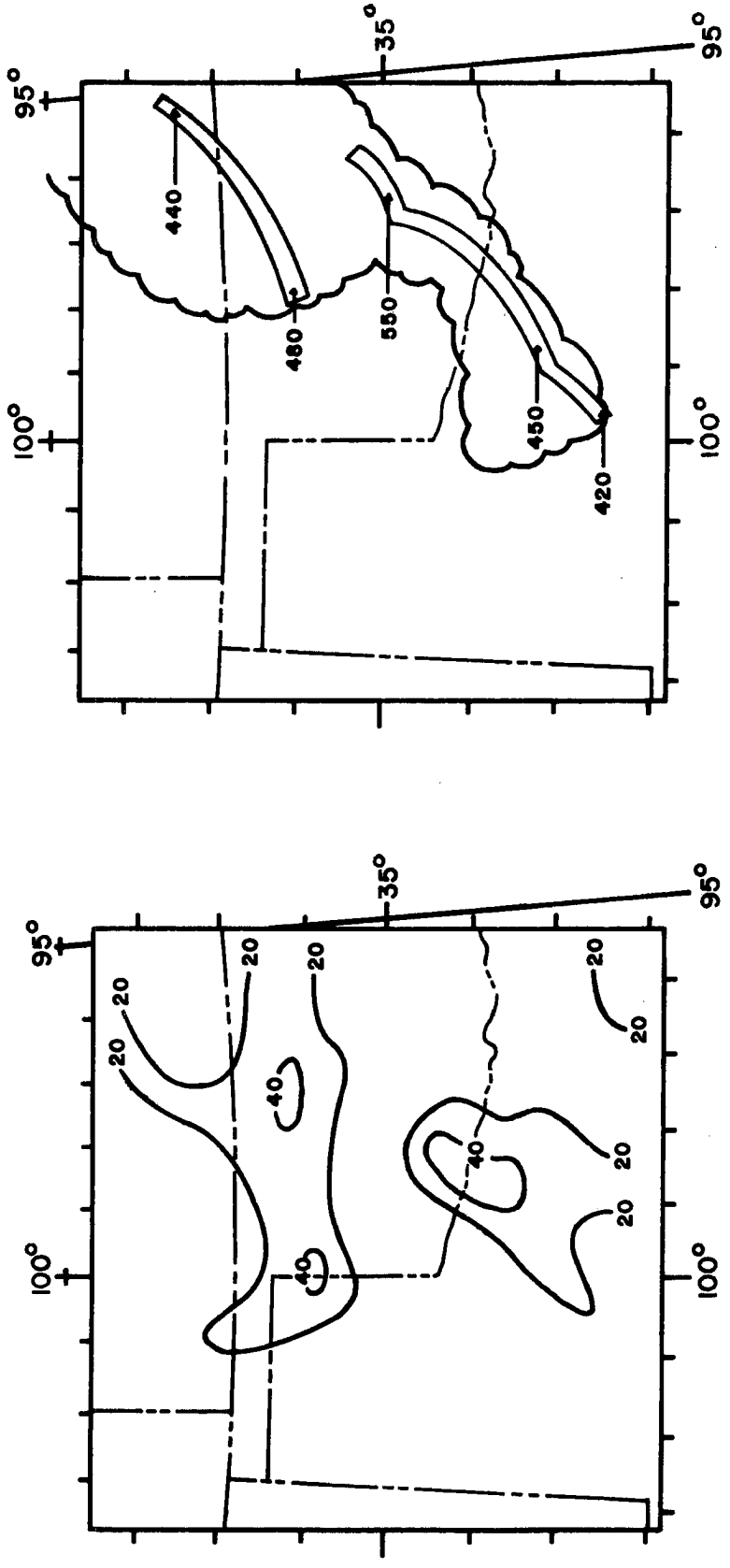

a) Surface moisture convergence (10^{-5} g kg^{-1} s^{-1}) 19 April 1972 1800 CST.

b) NWS radar summary 19 April 1972 1945 CST.

Figure 3-7 (from Sasaki, 1973).

and Maddox et al., 1977) showed that identifiable maxima in the moisture convergence field may precede development of intense convection by as much as 2-3 hours.

3.3.1 Moisture convergence using satellite derived precipitable water

On 24 April 1975, Vertical Temperature Profile Radiometer (VTPR) data was taken by the polar orbiting NOAA-4 satellite. This uses the 15 μm CO_2 channels for temperature retrieval and the rotational water vapor absorption band to infer precipitable water (PW) values (Hillger and Vonder Haar, 1976). This section explores the possibility of combining the satellite derived wind and moisture fields to simulate data that will become available with the launch of the VISSR* Atmospheric Sounder (VAS) on a geosynchronous satellite in the 1980's. A mesoscale moisture analysis is combined with the satellite derived winds to allow for the computation of moisture convergence in the boundary layer for the pre-storm environment.

The moisture analysis at 1616 GMT was available in terms of total precipitable water values at a resolution of ~70 km. The conventional radiosonde network would provide similar data at a resolution of about 400 km. Figure 3-8 shows the derived PW field. An iterative retrieval program (Hillger and Vonder Haar, 1977) retrieves temperatures (and moisture) in mostly clear columns of the atmosphere. High clouds (above 500 mb) in central Kansas caused the PW values to be too low. Otherwise, the individual values should be accurate to within ±0.5 cm of precipitable water.

This moisture field was then objectively analyzed in the manner of the 1800 GMT winds and the horizontal moisture divergence (MD) was

*Visible and Infrared Spin Scan Radiometer

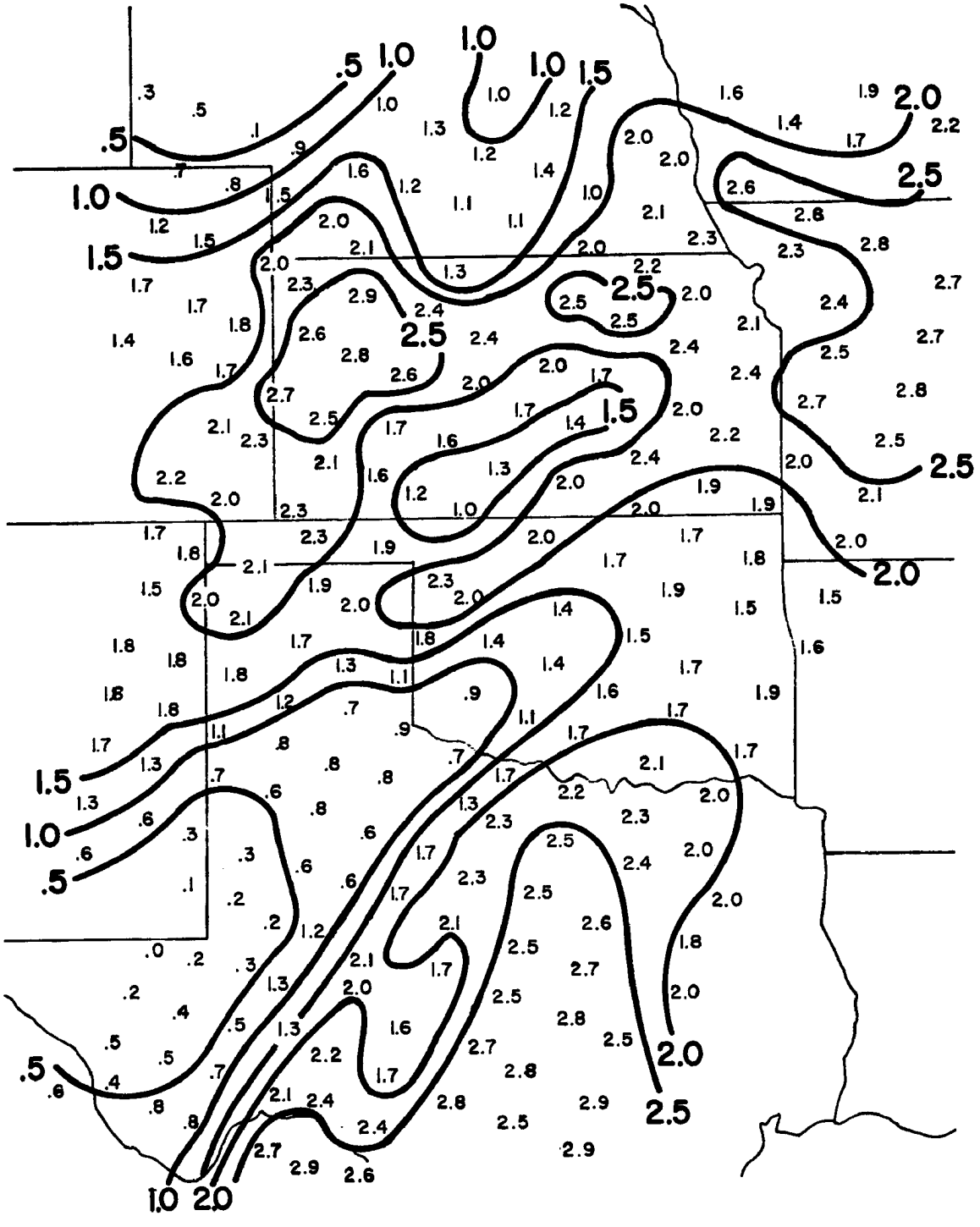

Figure 3-8 Satellite derived precipitable water field (cm) at 1615 GMT (from Hillger and Vonder Haar, 1977).

calculated at each grid point:

$$MD = \nabla \cdot (PW\ V) \tag{3-1}$$

where PW is the precipitable water (cm) and V is the velocity vector. The significance of this term can be best understood by using the vector identity:

$$\nabla \cdot (MV) = V \cdot \nabla M + M(\nabla \cdot V) \tag{3-2}$$

where M is a moisture dependent variable (mixing ratio, precipitable water, dew point) and V is the velocity.

The expression tends to have large negative values under conditions of:

1. advection of moist air [$V \cdot \nabla M < 0$] and
2. horizontal convergence [$M(\nabla \cdot V) < 0$].

Moisture convergence is thus a measure of both the inflow of moist air and of the low-level convergence needed to create upward vertical motion. The moisture divergence field is illustrated in Figure 3-9. Only negative values (moisture convergence) have been contoured. The maximum moisture convergence was ~30 x 10^{-5} cm H_2O s^{-1} centered in eastern Kansas. Local maxima are also found in southern Missouri, western Oklahoma, central Texas, and northern Louisiana. The radar summary at 1835 GMT (Figure 3-10) shows some convective activity occurring in Kansas; however, these storms were not severe.

There is a rather large time discrepancy between the moisture field (1600 GMT), the wind field (1800) and the time of initial storm genesis (2200). Because of this, emphasis in this section has been placed on the description of a technique, rather than on demonstrating the possible correlation between moisture convergence and the occurrence of

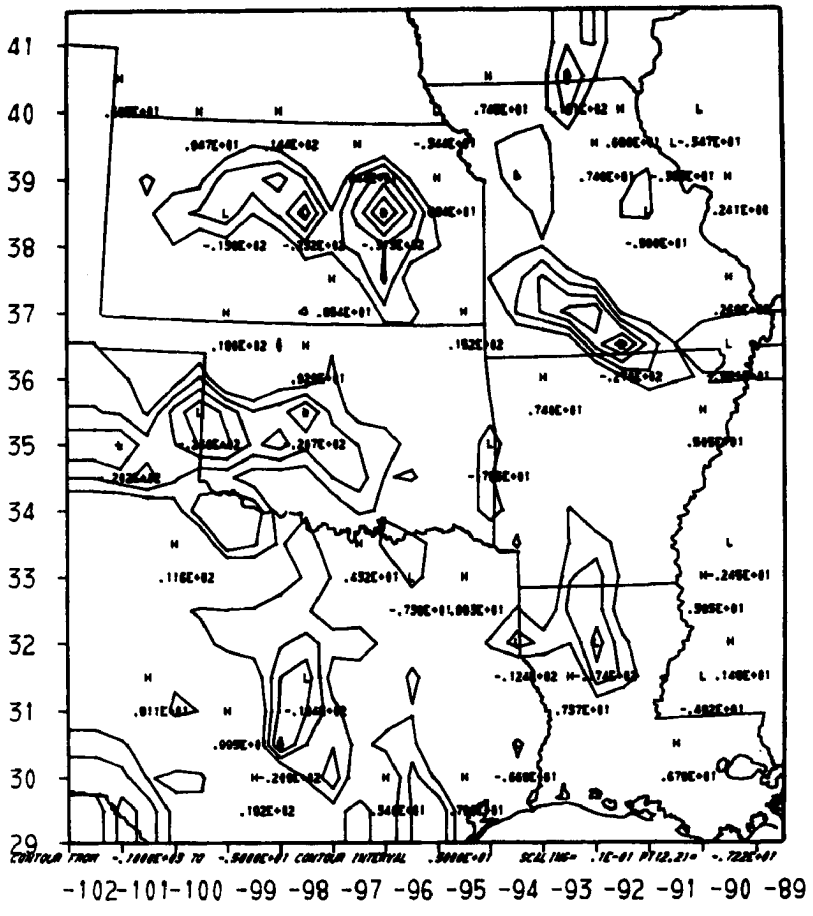

Figure 3-9 The moisture divergence field at 1800 GMT. Only negative values (moisture convergence) have been contoured. Units are cm H_2O s^{-1} x 10^{-5}.

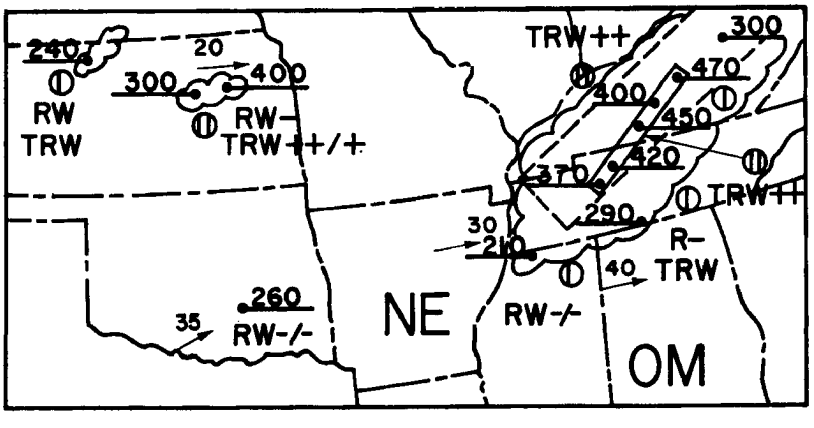

Figure 3-10 NWS radar summary at 1835 GMT.

severe local storms. The next section will use the technique to couple the 2100 GMT derived winds with corresponding surface mixing ratios to determine possible correlations. It has been stressed here, however, that using data from satellite sensors alone, wind and moisture fields can be constructed and combined to give mesoscale horizontal moisture flux information. A proposed vertical temperature sounder, placed on a geosynchronous satellite, will provide a vital tool for the implementation and evaluation of this technique, notably as a real time "now-cast" forecasting aid.

3.3.2 Moisture convergence from surface mixing ratios

Surface mixing ratios were computed from the 2100 GMT surface observations using the definitions of mixing ratio and Teten's empirical formula for vapor pressure:

$$q_s = 0.622 \frac{e_s(T)}{p - e_s(T)} \tag{3-3}$$

$$e_s(T) = 610.78 \exp[\frac{17.269(T - 273.16)}{T - 35.86}] \tag{3-4}$$

where: q_s is the saturation mixing ratio

e_s is the saturation vapor pressure

P is the (surface) pressure

The saturation vapor pressure (e_s) is in Pascals (Pa) when the temperature is in °K. The mixing ratio (q) is then computed using the dew point temperature (T_d). The resultant field of $\nabla \cdot (qV)$ is presented in Figure 3-11. Units are g $kg^{-1}s^{-1}$ x 10^{-5}. Comparison with Figure 3-12 shows that during the following 2 hours storms developed in most regions characterized by large values of moisture convergence at 2100 GMT. The

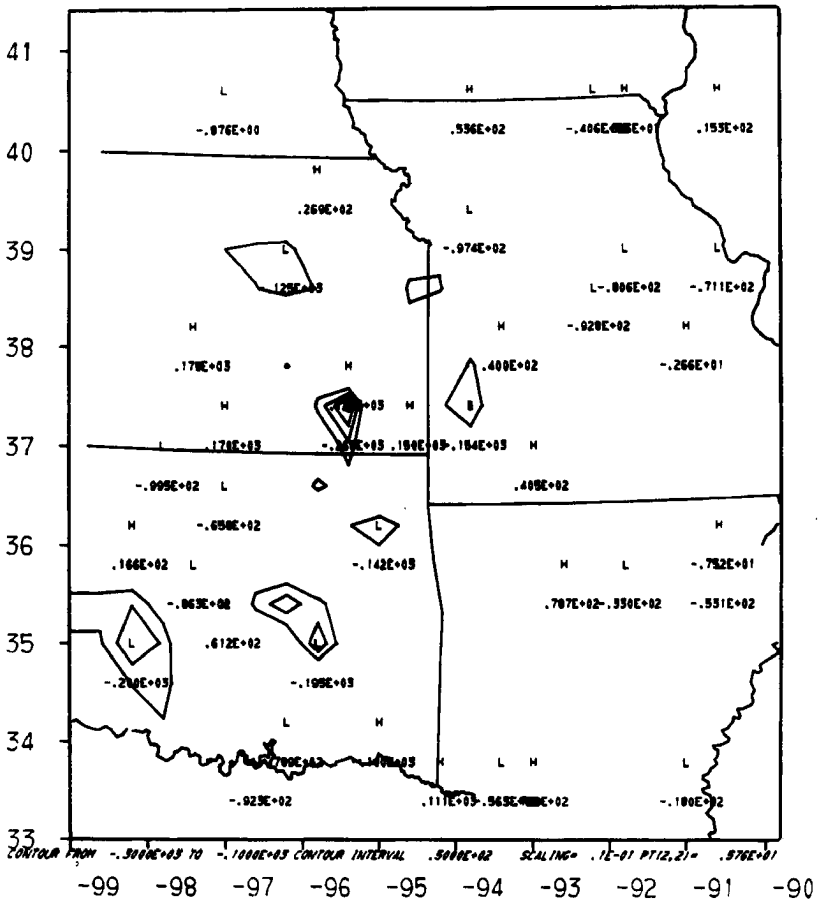

Figure 3-11 2100 GMT moisture divergence field using satellite derived winds and surface mixing ratios. Only negative values (moisture convergence) have been contoured. Units are g $kg^{-1}s^{-1}$ x 10^{-5} and contour interval is 50 x 10^{-5} g $kg^{-1}s^{-1}$.

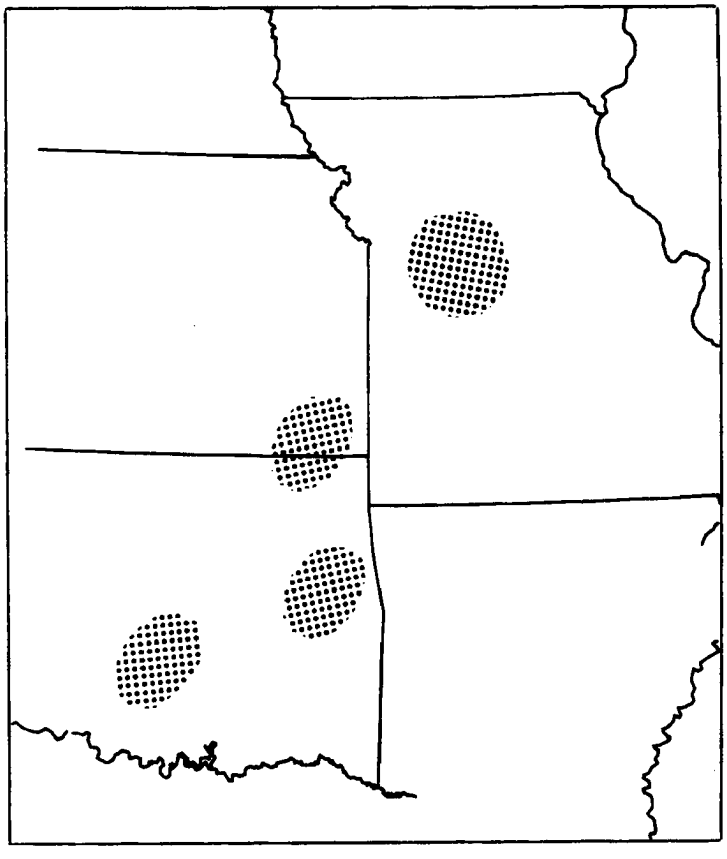

Figure 3-12 Severe storm locations at 2300 GMT.

main exception was the lack of activity within the convergence region in central Kansas. A reexamination of the original wind field (Figure 3-4) shows that almost no wind vectors are found in that area, so the validity of the gridded winds there are questionable. Maximum values of moisture convergence (~2.2 x 10^{-3} g $kg^{-1}s^{-1}$) are similar to values found by Sasaki (1975) to be associated with severe thunderstorm occurrences. The Neosho, Missouri tornadic storm began to develop within an hour of the satellite measurements and within the area of highest moisture convergence. The same field using only 2100 GMT surface winds is shown in Figure 3-13. The overall pattern of the two fields is similar, however, the surface based analysis indicates moisture divergence over much of south and southcentral Oklahoma. This is an important difference since several severe storms developed across that region. There are also areas of moisture convergence where no severe weather occurred. An improved correspondence between maximum moisture convergence and subsequent severe storm genesis was characterized by the satellite field. Elimination of local effects on surface winds and a stronger flow at cloud base are postulated as the cause.

3.4 Dynamic Parameters

3.4.1 The divergence term

Wilson (1976) has computed large-scale vertical motion fields using the Atmospheric Variability Experiment (AVE IV) sounding data collected on 24 April. His computations showed that the large-scale vertical motions did not play a major role in organizing the convection on this day since the storms developed in regions of diagnosed synoptic scale subsidence or of only slight upward motion (refer to Figure 2-6). Therefore, these storms were induced by mesoscale processes. Endlich and

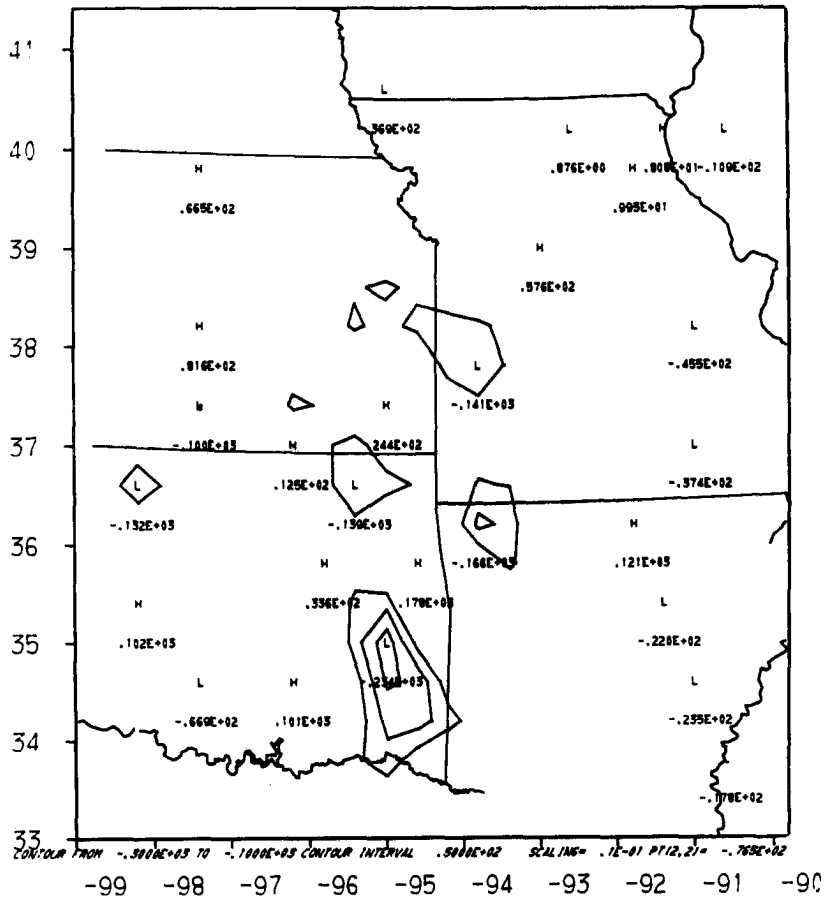

Figure 3-13 2100 GMT moisture divergence field using observed surface winds and mixing ratios. Units and contour interval are the same as in Figure 3-11.

Mancuso (1968) showed that the term for vorticity production in the vorticity equation was a good objective indicator of severe storm activity. The vorticity equation in Cartesian coordinates is:

$$\frac{d}{dt}(\zeta+f) = -(\zeta+f)\left(\frac{\partial u}{\partial x} + \frac{\partial v}{\partial y}\right) - \left(\frac{\partial w}{\partial x}\frac{\partial v}{\partial z} - \frac{\partial w}{\partial y}\frac{\partial u}{\partial z}\right) + \frac{1}{\rho^2}\left(\frac{\partial \rho}{\partial x}\frac{\partial p}{\partial y} - \frac{\partial \rho}{\partial y}\frac{\partial p}{\partial x}\right) \qquad (3\text{-}5)$$

where ζ is the relative (parcel) vorticity

f is the Coriolis (earth) vorticity

u,v,w are the components of the velocity vector

ρ is the density.

Equation (3-5) states that the rate of change of the absolute vorticity following the motion is given by the sum of the three terms on the right, called the divergence term, the tilting term and the solenoidal term respectively. Using Doppler wind information, Ray et al. (1976) found the tilting term to be an order of magnitude smaller than the divergence team. Scale analysis (Holton, 1972) shows the solenoidal term can also be neglected.

From the definition of relative vorticity (ζ) and divergence (D) in finite difference form:

$$\zeta = \frac{\Delta v}{\Delta x} - \frac{\Delta u}{\Delta y} \qquad (3\text{-}6)$$

$$D = \frac{\Delta u}{\Delta x} + \frac{\Delta v}{\Delta y} \qquad (3\text{-}7)$$

and keeping the value of f constant (0.875×10^{-4} at 37°N) we can write the production of vorticity due to divergence as:

$$\frac{d\zeta}{dt} = -D(\zeta + f) \qquad (3\text{-}8)$$

For mesoscale systems ζ cannot be neglected with respect to f as is often done in synoptic scale computations. The field of "vorticity production" is shown in Figure 3-14. Units are $s^{-2} \times 10^{-9}$ and only positive values are contoured. Comparison with Figure 3-12 shows a significant correspondence exists between areas of high mesoscale vorticity production and the subsequent occurrence of severe local storms. It appears that values on the order of $15 \times 10^{-9} s^{-2}$ are necessary and sufficient to force the occurrence of severe weather.

3.4.2 Relative vorticity

The field of relative vorticity (ζ) alone can provide some clue as to severe storm genesis, as well as provide an insight into the sensitivity of the data set to the density and number of wind vectors. Figure 3-15 is the 2100 GMT relative vorticity computed using finite differencing on the satellite derived wind field. The vorticity is concentrated in a narrow band along the front and dry line as would be expected. Maximum values of $2 \times 10^{-4} s^{-1}$ are of the order of the earth's vorticity at that latitude. A subjective modification was made to the original data set such that eleven vectors near the rear of the fronts were arbitrarily deleted. The modified field is shown in Figure 3-16. The results differ in both general pattern and by as much as two orders of magnitude in some regions. The modification was made to maximize differences; however, the ability to track small cumulus is dependent on real weather systems. It is often impossible to find cumulus clouds behind a dry line, and low-level clouds are often obscured by layers of middle and high clouds to the north of a surface front. The Neosho, Missouri tornadic storm developed in an area of a local maximum of relative vorticity. While the concentration of vorticity for tornado

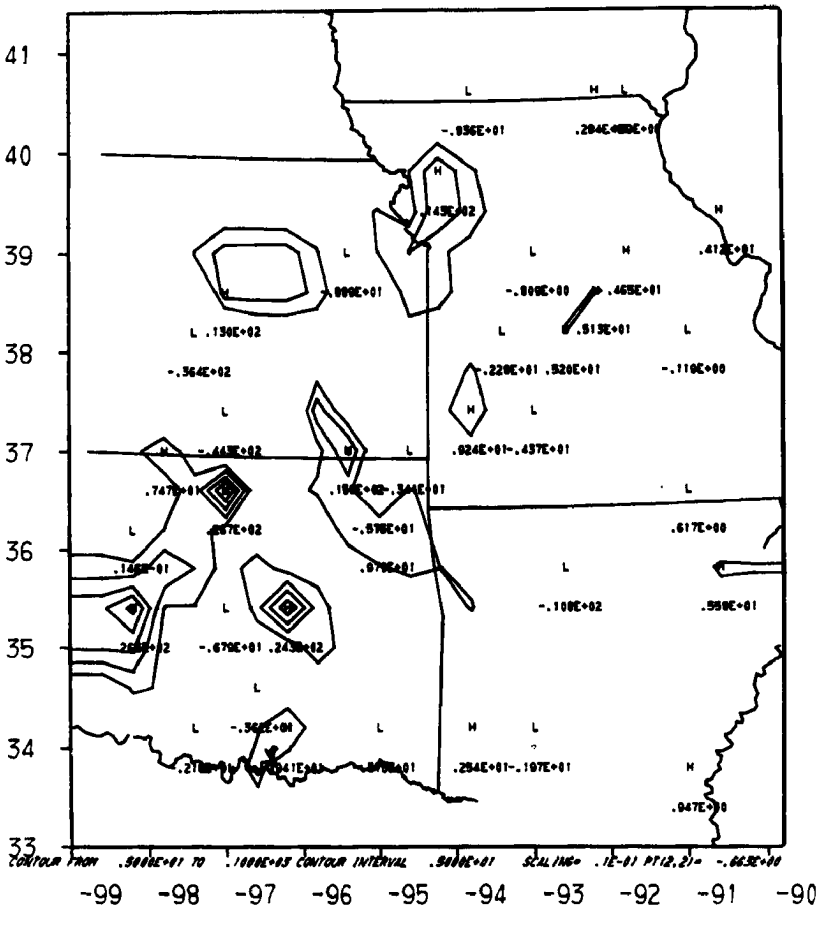

Figure 3-14 "Vorticity production" at 2100 GMT. Only positive values have been contoured. Units are $s^{-2} \times 10^{-9}$ and contour interval is 5×10^{-9} s^{-2}.

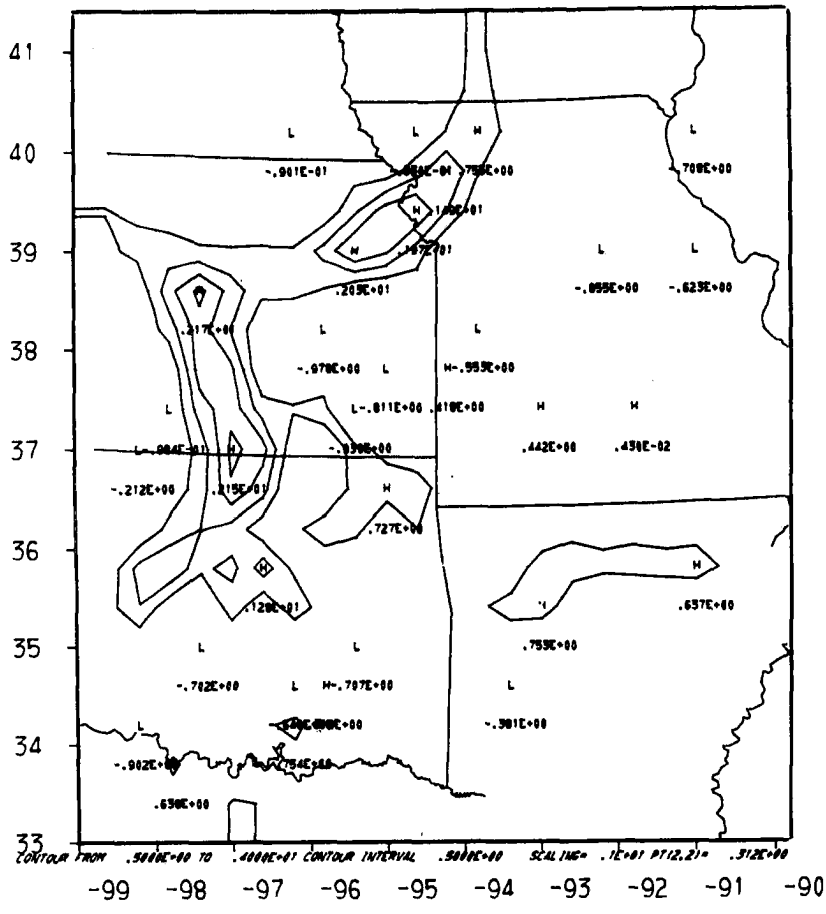

Figure 3-15 Relative vorticity computed from satellite derived winds at 2100 GMT. Only positive values have been contoured. Units are $s^{-1} \times 10^{-4}$ and contour interval is $5 \times 10^{-5}\ s^{-1}$.

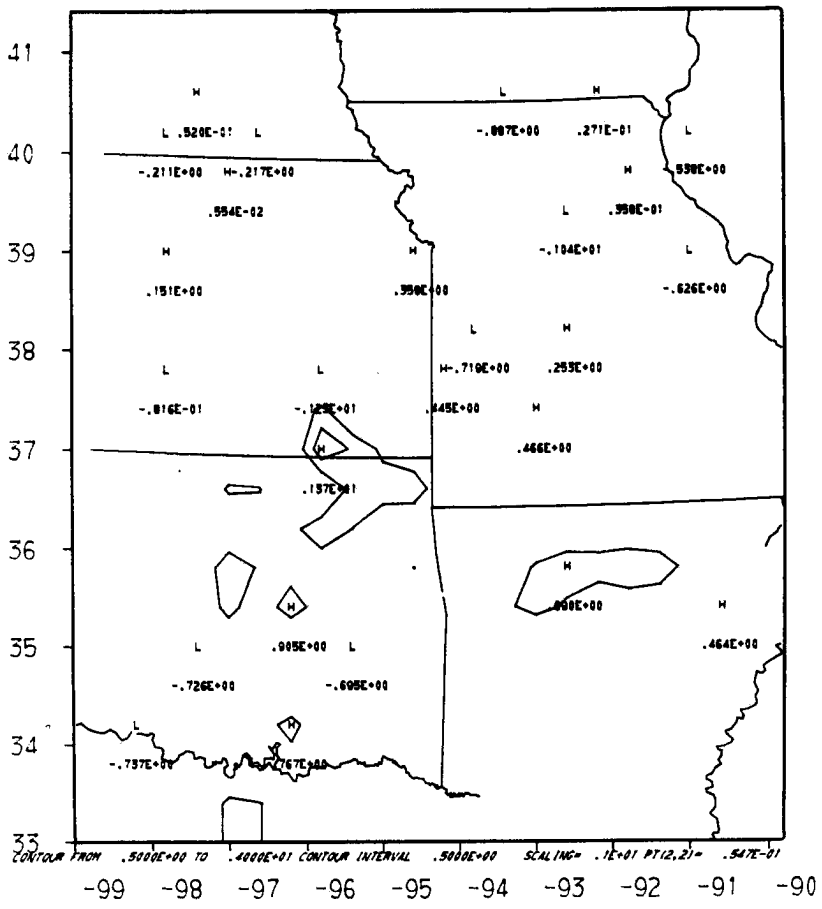

Figure 3-16 Relative vorticity computed from the modified satellite derived winds. Details are as in Figure 3-15.

genesis is on a scale smaller than the mesoscale, the satellite derived field indicates a high vorticity environment was present at the outset.

3.5 Summary of Wind and Moisture Fields

This chapter has detailed some of the computations that can be made using satellite derived wind fields. Using data from satellite sensors alone, horizontal moisture flux information can be obtained. Because of the early NOAA-4 pass time, and a 2-hour discontinuity between the wind and moisture fields, no inferences were made to the correlation of low-level moisture convergence and the occurrence of severe local storms at 1800 GMT. Using 2100 GMT surface mixing ratios as the moisture parameter, however, subsequent severe storm development occurred within several of the regions of diagnosed high moisture convergence. Satellite moisture convergence patterns specified convective patterns that developed better than did the same field computed using only surface observations. This suggests that satellite data may be useful in operational severe storm forecasting. Several dynamic parameters (vorticity production, relative vorticity) can also be used as good indicators of severe storm potential. Table 3-2 summarizes the results of this and previous studies.

3.5.1 Limitations

The author is well aware of the limitations of the technique described. One such limitation is the fact that the satellite winds are not exactly located in the vertical. Schaefer (1973) pointed out that when divergence is computed on a non-horizontal surface, additional terms appear in the defining equation. Consider (x,y,z) as the spatial coordinates in a constant height system and (x,y,p) as the spatial coordinates in a constant pressure system. The formula for transferring

Table 3-2. Previous Studies of Severe Weather-Related Parameters

Investigator	Scale	Divergence (s^{-1})	Relative Vorticity (s^{-1})	Moisture Divergence	Vorticity Production (s^{-2})
Endlich and Mancuso, 1968	synoptic			-20×10^{-5}[°C s^{-1}]	30×10^{-10}
Viezee et al., 1972	synoptic		2×10^{-5}		
Sasaki, 1973	mesoscale	-5×10^{-5}		-40×10^{-5}[$gkg^{-1}s^{-1}$]	
Hougton and Wilson, 1975	mesoscale	-5×10^{-5}			
Ostby, 1975	mesoscale			-150×10^{-5}[$gkg^{-1}s^{-1}$]	
Suchman and Martin, 1976	mesoscale	-6×10^{-5}			
Peslen, 1977	mesoscale	-8×10^{-5}	$10^{-5} - 10^{-4}$		
Maddox et al., 1977*	mesoscale		2×10^{-4}	-200×10^{-5}[$gkg^{-1}s^{-1}$]	
Negri et al., 1977*	mesoscale	-10×10^{-5}		-20×10^{-5}[cm H_2O s^{-1}]	
Present study	mesoscale	-10×10^{-5}	2×10^{-4}	-200×10^{-5}[$gkg^{-1}s^{-1}$]	200×10^{-10}

*Same data set as present study.

the divergence from one system to another is given by:

$$D = (\nabla_H \cdot V)_z = (\nabla_H \cdot V)_p - \frac{\partial v}{\partial z} \cdot (\nabla_H z)_p \qquad (3\text{-}9)$$

This states that the divergence on a surface of constant height equals the difference between the divergence on a surface of constant pressure and the product of the vertical wind shear and the slope of the height surfaces. For this case, it was assumed that the satellite winds were on a horizontal surface, even though rawinsonde data indicated that the LCL (lifted condensation level, an estimate of cloud base) ranged from 910 to 800 mb across the region in question. For small vertical wind shears and gentle slopes (last term in (3-9) $<< 10^{-5} s^{-1}$) the simplifying assumptions remain valid. Other limitations include the fact that the 1800 GMT wind fields were multiplied by an estimation of the <u>total</u> atmospheric water content, not just boundary layer moisture. Total precipitable water content is likewise not retrieved perfectly. It was also shown that the derived fields are sensitive to the density and spatial configuration of the original wind fields, and most likely sensitive as well to the objective analysis scheme used. Satellite derived winds lend themselves to processing by multi-variate analysis, which would simultaneously analyze satellite winds, surface and upper air data, and other data in the best possible way to reduce error.

4.0 SATELLITE MONITORING OF SEVERE LOCAL STORMS

4.1 Previous Studies

It was shown in the last section how monitoring of the pre-storm environment through the use of satellite derived convergence patterns could give an indication of subsequent severe storm genesis areas. Equally, or perhaps more important, is the continued observation of these areas by a geosynchronous satellite having high temporal frequency. Satellite measurements in the atmospheric "window" (10-12 μm) can differentiate between convective elements of differing duration and intensity. One may then deduce the intensity of this convection and then (hopefully) be able to discriminate between severe and non-severe elements.

Previous attempts using satellite infrared (IR) data have largely been qualitative and have relied on the use of enhanced IR imagery. Purdom (1976a) used rapid interval high resolution GOES imagery to view tornadic storms from both an earth relative frame and a thunderstorm relative frame. He concluded that a relative low-level south to southeast cloud flow into a severe storm is important in that storm's ability to produce a tornado. Purdom (1976b) has also observed the presence of a variety of trigger mechanisms and interactions that range in scale from the synoptic to the mesoscale. Among such mechanisms that exert a strong influence on the initiation and maintenance of thunderstorms are convective lines, convective cloud mergers, and convective line intersections, all visible on satellite imagery. Oliver and Scofield (1976) and Scofield and Oliver (1977) present schemes for estimating convective rainfall from satellite visible and IR imagery. The major assumptions of their scheme are summarized in Table 4-1. While this present study

Table 4-1. Convective Rainfall Estimation Scheme (from Scofield and Oliver, 1977)

1. Bright clouds in the visible imagery produce more rainfall than darker clouds.

2. Bright clouds in the visible and clouds with cold tops in the IR imagery which are expanding in areal coverage (in early and mature stages of development) produce more rainfall than those not expanding.

3. Decaying clouds produce little or no rainfall.

4. Clouds with cold tops in the IR imagery produce more rainfall than those with warmer tops.

5. Clouds with cold tops that are becoming warmer produce little or no rainfall.

6. Merging of cumulonimbus (Cb) clouds increases the rainfall rate of the merging clouds.

7. Most of the significant rainfall occurs in the upwind (at anvil level) portion of a convective system. The highest and coldest clouds form where the thunderstorms are most vigorous and the rain heaviest. These cold clouds get thinner downwind and look warmer in IR imagery as the anvil material blows away from its origin.

does not address itself specifically to the determination of convective rainfall amount, several of the assumptions of Table 4-1 can be applied to the detection of severe thunderstorms.

Other authors took the next step toward a more quantitative approach to the remote sensing of convection. Arn (1975) used the Optical Data Digitizer and Display System (OD^3) to digitize film loops from the third Applications Technology Satellite (ATS-3) and from the second synchronous meteorological satellite (SMS-2). He analyzed visible channel radiances ("brightness") from the anvils of severe thunderstorms in an attempt to discern signatures which would describe storm severity. Among the parameters found useful were anvil area divergence (1/A dA/dt), area speed gradients (d^2A/dt^2), and volume flux (dVo/dt). Griffith et al. (1976) used a densitometer to examine ATS visible images. They found that daily rainfall in the tropics could be estimated from cloud brightness, a technique which is currently being tested in the mid-latitudes.

Perhaps the most quantitative method of observing severe storm characteristics is through the use of the original satellite digital data itself. Auvine and Anderson (1972) obtained upper tropospheric fluxes and divergence for several storms from measurements of anvil area expansion. They presented two models based on the point source concept of a growing cumulonimbus anvil. These models are reproduced in Figure 4-1, and conform well with actual observations of anvil shape and expansion. Adler and Fenn (1976, 1977) have developed techniques to use high frequency SMS infrared data to help detect and monitor severe thunderstorms. This study will use some of their techniques in an attempt to discriminate between severe and non-severe storms from the vantage point of a satellite platform. Adler and Fenn showed that three

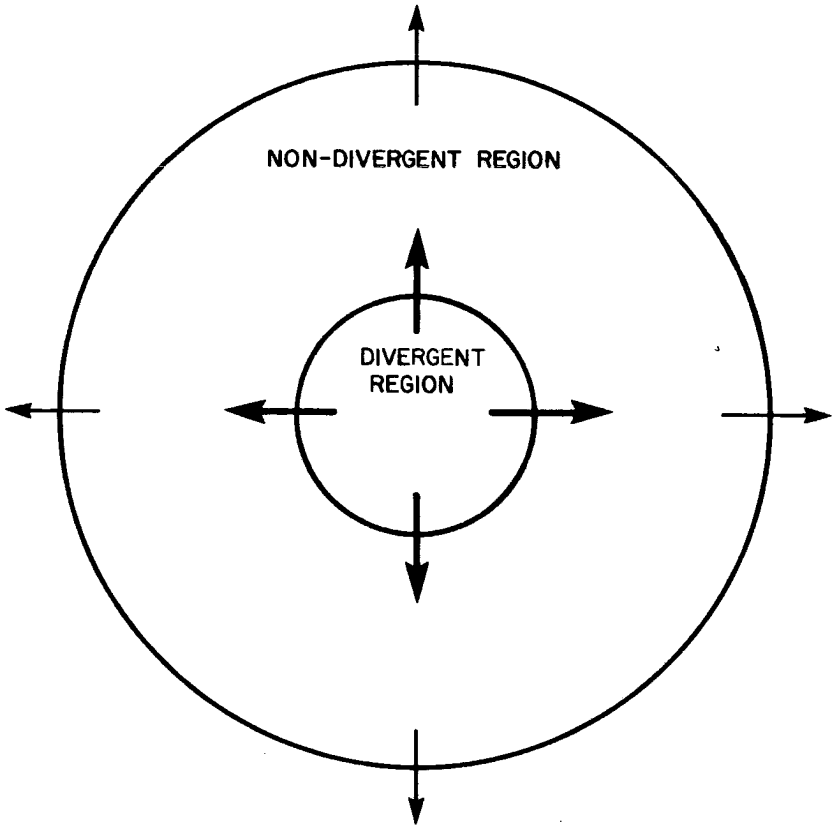

a) A model of airflow within the thunderstorm anvil assuming calm environmental winds.

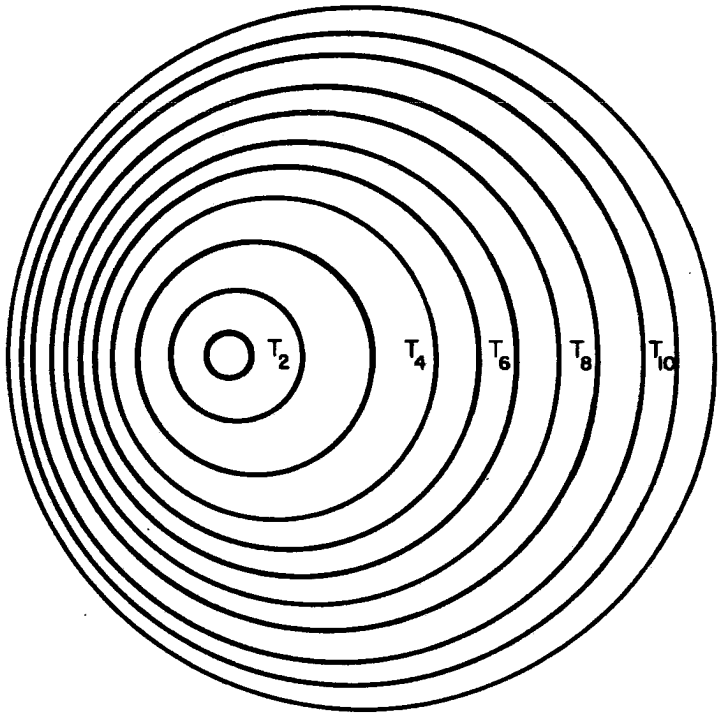

b) The material outline of a cumulonimbus anvil assuming its growth to be the result of a point source in a uniform stream.

Figure 4-1 Thunderstorm anvil models (from Auvine and Anderson, 1972).

simple characteristics seemed to be correlated with the occurrence of severe weather. These are duration, minimum cloud top temperature, and cold area rate of increase. The following sections will examine these characteristics for the storms of 24 April 1975, after a brief look at the theory of remote sensing.

4.2 Radiative Transfer Equation

In the spectral interval 10-12 μm, the clear atmosphere is essentially a non-scattering, non-absorbing medium. Thus, the equation of radiative transfer reduces to:

$$N(\lambda) = B(\lambda, T)\tau\varepsilon \tag{4-1}$$

where $N(\lambda)$ is the spectral radiance observed at the top of the atmosphere in a spectral interval $d\lambda$ around mean wavelength λ

τ is the transmittance at wavelength λ of any optically absorbing gas (assumed $\tau = 1$ for $\lambda = 10\text{-}12$ μm)

ε is the surface or cloud top emissivity (assumed $\varepsilon = 1$).

The Planck blackbody radiance $B(\lambda, T)$ at mean wavelength λ and temperature T is

$$B(\lambda, T) = \frac{c_1 \lambda^{-5}}{e^{c_2/\lambda T} - 1} \tag{4-2}$$

Thus, the temperature at which the top of a cloud radiates may be expressed as an effective blackbody temperature (T_{BB}) which can be continuously monitored by an infrared radiometer on a geosynchronous satellite.

4.3 Data and Methods

SMS digital visible and infrared data were obtained for the period 1800-0200 GMT on 24-25 April 1975. During this period the satellite was in a limited scan mode, wherein a small north-south segment is observed on a frequent basis (nominally five minutes). Data coverage on this time scale is necessary for severe storm monitoring when one considers the lifetime of most convective elements is less than 30 minutes. The clouds examined in this study are shown in the 2242 GMT infrared image of Figure 4-2. Clouds designated by names or numbers became severe storms, while the non-severe storm clouds are lettered. Visible channel data were not quantitatively examined due to low solar zenith angles during storm lifetimes.

The spatial resolution of the IR instrument is approximately 32 km^2 at nadir. Due to sampling constraints, however, IR "pixels" or scan spots were sampled twice in the east-west direction. Thus, each IR element referred to in later sections represents a mean area of ~90 km^2 at 40° north latitude. Infrared growth rates and temperatures are examined in an attempt to:

1. discriminate between severe and non-severe elements, and
2. link signatures in the IR data to the occurrence of severe weather on the ground.

This study will follow techniques initially used by Adler and Fenn (1976, 1977) to portray SMS infrared data in a temporal sequence. This was done to promote consistency in examining digital data as well as to facilitate the direct comparison of results. Starting at the cold end of the temperature spectrum, a cumulative histogram of data at or below a given temperature is compiled. That is, the number of points N_i,

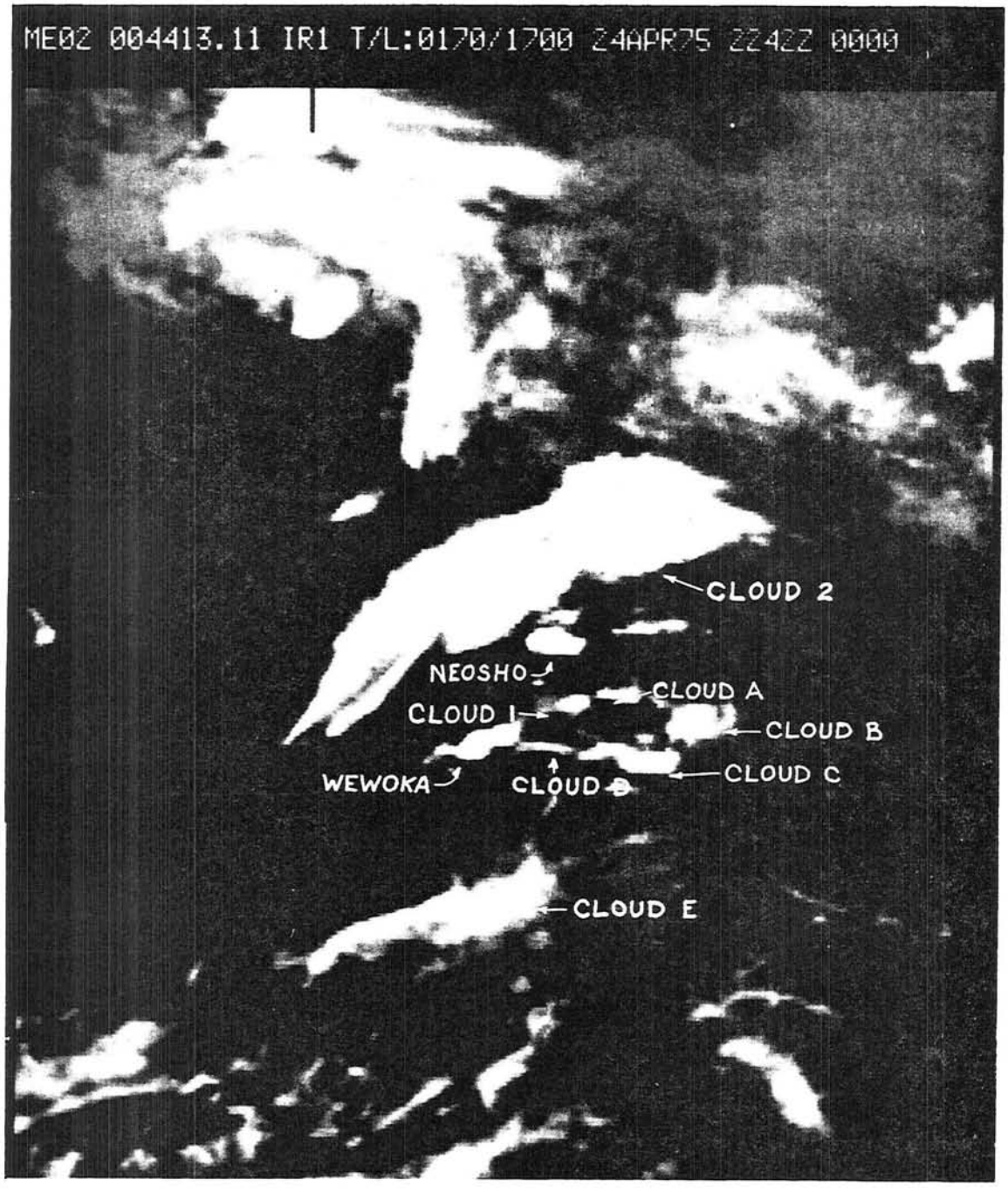

Figure 4-2 SMS-2 infrared image at 2242 GMT.
Cloud examined in this study are labelled.

with blackbody temperature $T_{BB} \leq T_i$ is obtained. The temperatures (T_i) range from the coldest temperature present to the warmest temperature, T_o, which is unambiguously part of the cloud. This temperature (T_o) is defined such that its contour is far enough within the cloud to avoid the effects of lower emissivity at the anvil edge. (An exception to this procedure for weak convective clouds will be investigated later.) When the warmer temperature contours near the edge of the anvil merge with the anvils of other storms, the warmest valid temperature (T_o) decreases. Late in the lifetimes of the storms, only the very cold areas are followed and thus only a small range of T_{BB} exist. Due to the method of data reduction utilized, the T_{BB} values represent a mean value of temperature over a 4°C interval. When applied in a consistent manner, this will not introduce significant error into the derived rates of growth. Rather than display the contour of every T_{BB}, representative temperatures were chosen to portray a wide range of anvil area. Particular attention, however, was given to the very cold portions of the cloud top (206-214 K), as they are often indicators of intense convection below.

4.4 Results for Severe Storms

Four of the clouds examined on this day produced tornadoes and/or large hailstones. Three of those storms will now be examined in detail: the Wewoka hailstorm, the Neosho tornadic storm and cloud no. 1, a hail producer (refer to Figure 4-2).

4.4.1 Wewoka

Figure 4-3 is the growth rate diagram for the cloud that produced baseball-sized hail over the town of Wewoka, Oklahoma. The graph displays the relationship between the number of data points, N_i, and time.

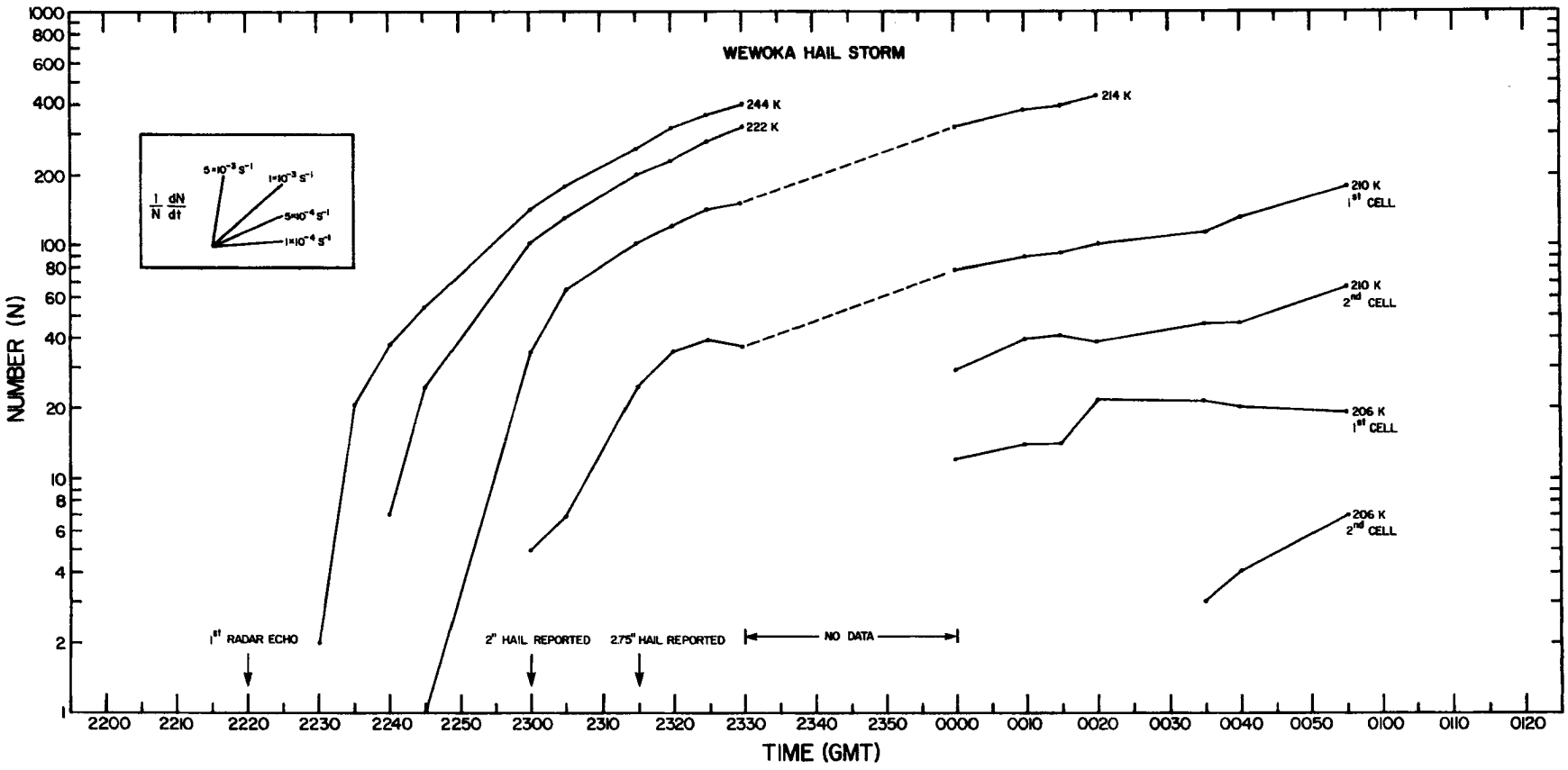

Figure 4-3 Thunderstorm growth rate diagram for the Wewoka hailstorm. N is the number of data points in the element with blackbody temperature $T_{BB} \leq T_i$, where T_i is as identified in the diagram.

Again, N_i is the number of IR pixels in the cloud top with blackbody temperature T_{BB} less than or equal to T_i. For example, in Figure 4-3, the 222K isotherm, which contained 7 pixels (~630 km^2) at 2240 GMT, expanded to 21 pixels (~1890 km^2) in just five minutes. Because the ordinate of the graph is logarithmic, the slopes of the lines are proportional to $\frac{1}{N} dN/dt$. Adler and Fenn (1977) found that in seven of eight cases studied, the first report of severe weather occurred during, or just after, a rapid expansion of cold areas. It is worth noting that the Wewoka storm's coldest temperature (-67°C to -63°C) did not appear until two hours after the occurrence of hail. Thus, while the temperature at cloud top may indicate its convective potential in terms of rainfall (Scofield and Oliver, 1977), it is not necessarily a precursor to storm severity, i.e., tornadoes and large hail. Figure 4-4 illustrates the temporal changes in divergence and rate of decrease of cloud top minimum temperature for the Wewoka storm. The bottom portion represents the slopes of the family of curves of Figure 4-3. For example, the change in divergence of the 222K isotherm is found by following the open triangular symbols. Divergence values of $1\text{-}5 \times 10^{-3}$ s^{-1} are found in the pre-hail period, while much slower rates of $5\text{-}10 \times 10^{-4}$ s^{-1} are observed after the occurrence of hail. This order of magnitude difference is physically related to the vertical motion occurring under the cirrus anvil. The rate of change of minimum blackbody temperature (Figure 4-4, top) provides little insight as to the time of hail occurrence. An initial period of rapid decrease is followed by a period where temperature changes little with time. Minimum blackbody temperature was thus a poor indicator of the time of severe weather in this case; however, it will be shown that it is a good indicator of severe versus non-severe elements.

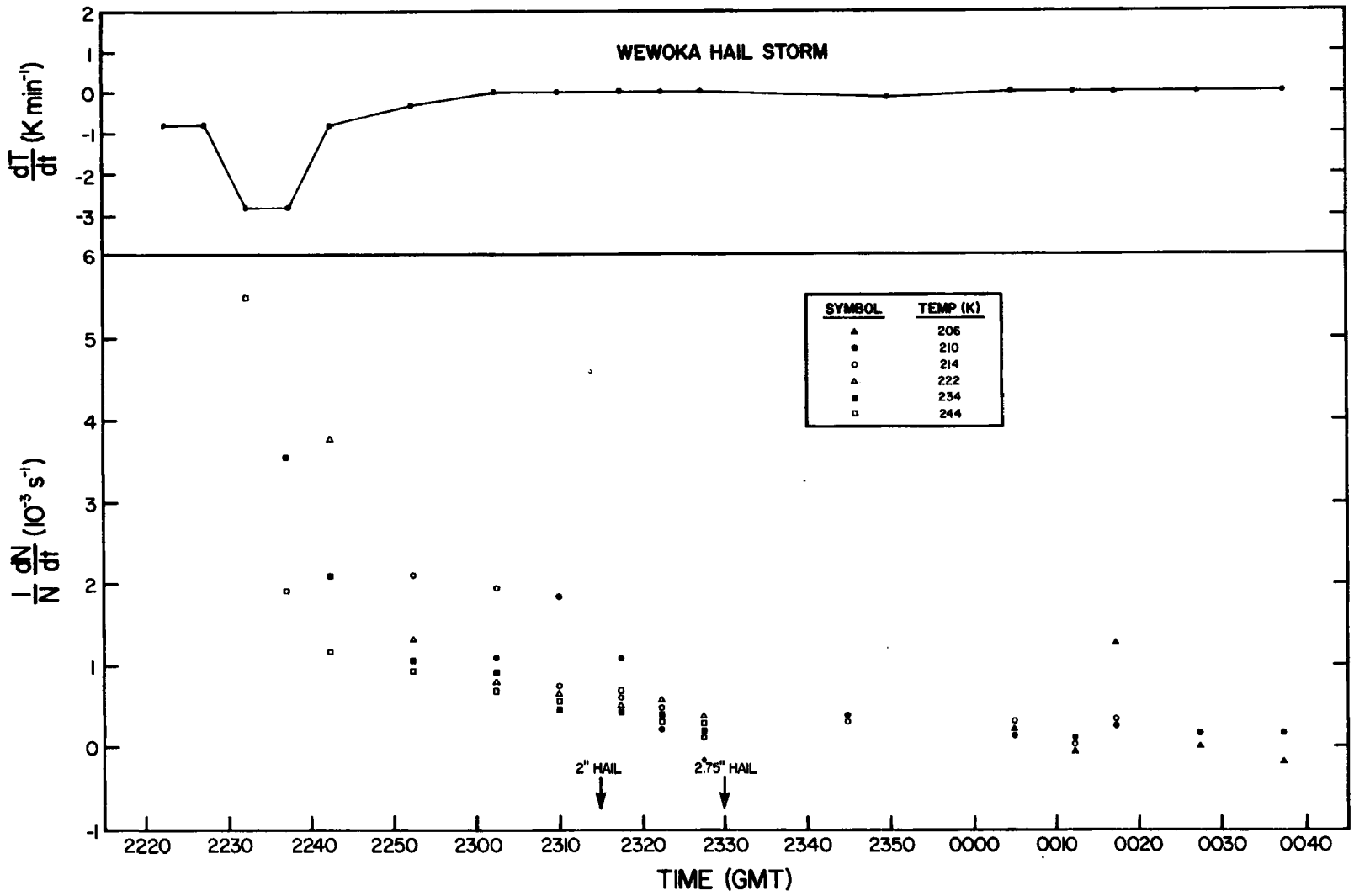

Figure 4-4 Temporal change in divergence and rate of decrease of cloud top minimum temperature (top) for the Wewoka storm.

4.4.2 Neosho

As viewed from the satellite, the Neosho storm was much less spectacular that the neighboring Wewoka storm. The growth of the Neosho storm, considerably less than the explosive growth of Wewoka, is shown in Figure 4-5. In this case, the rate of growth did not specify storm severity. The storm spawned tornadoes at Miami, Oklahoma, at 0010 GMT and at Neosho, Missouri, at 0040, nearly two hours after its inception. Studies by Fujita (1973) indicate a preference for the formation of stronger tornadoes later in the day. The analysis is also hampered by a lack of data between 2330 and 0000 GMT. While both reports of tornadoes occur during or following rapid cold area increases, the observations rest weakly on the basis of only several data points. The variation in divergence, and in rate of change of minimum temperature (Figure 4-6) also show very little in the way of identifiable signatures. Active convection near the time of the tornadoes was most likely obscured by the extensive cirrus anvil. Overshooting tops were apparent in the visible imagery, however. Fujita (1973) proposed a mechanism of tornado formation whereby the collapse of the overshooting top, due to precipitation overloading, induces a twisting downdraft inside of a rotating storm. Overshooting tops are not apparent in the IR channel due to its coarser resolution and finite response time. An overshooting tower rapidly becomes much colder that its environment as it overshoots and penetrates the tropopause. However, the storm tops entrain environmental air as they "boil" above the anvil. Because the environmental air temperature changes little with height, the net effect is the smoothing or masking of the presence of the very cold temperature within the cloud top.

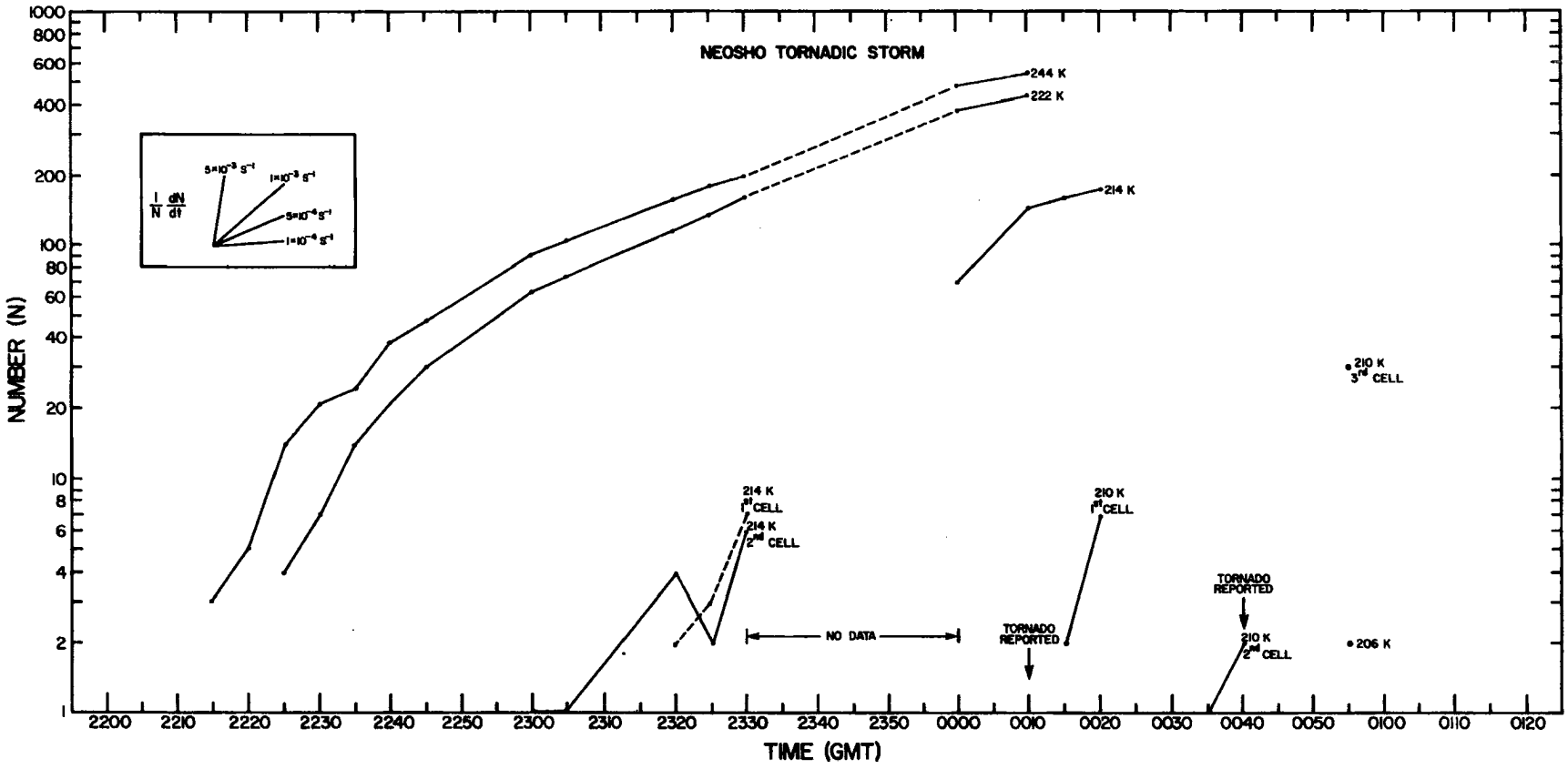

Figure 4-5 Thunderstorm growth rate diagram for the Neosho tornadic storm.

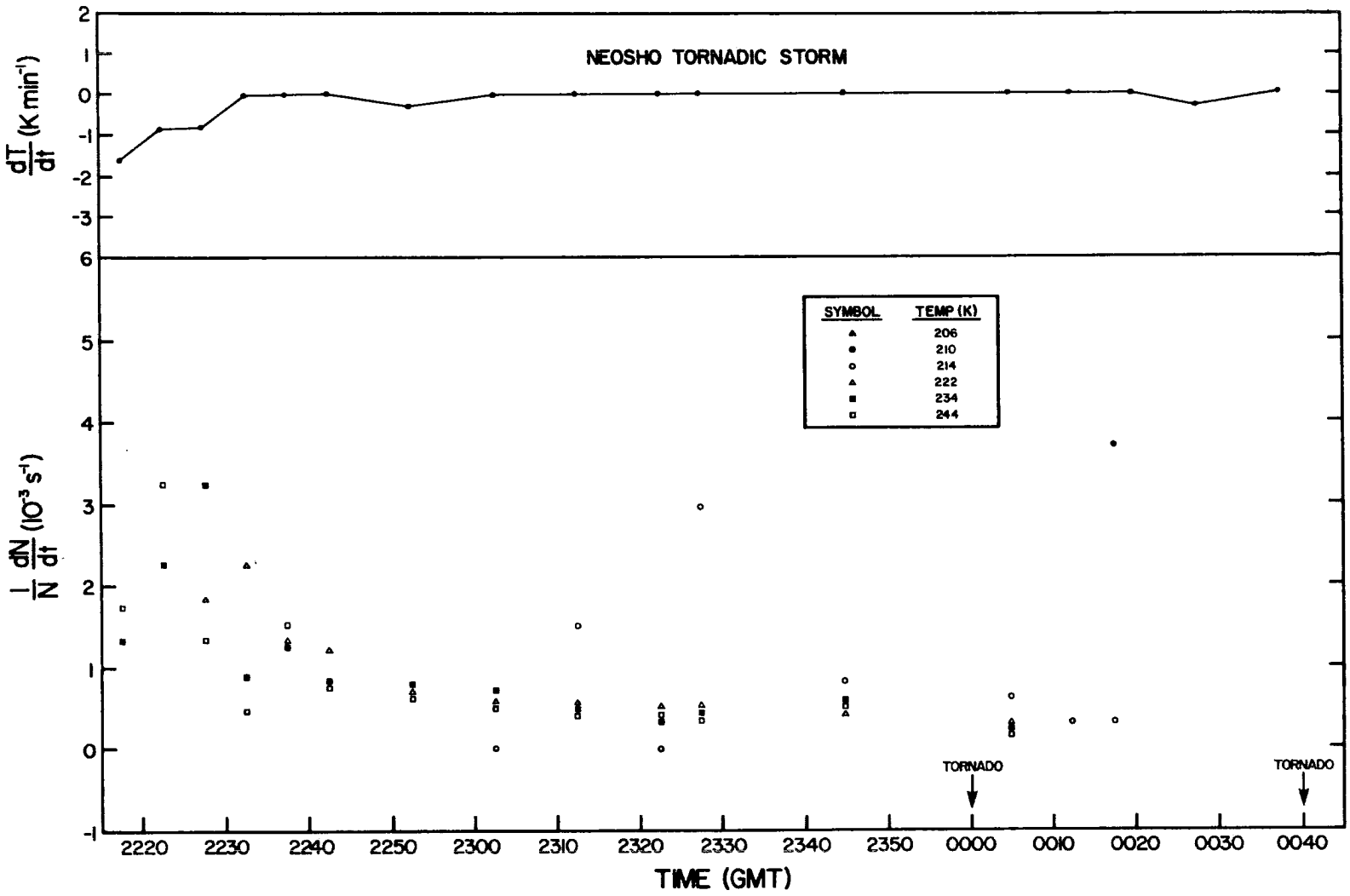

Figure 4-6 Temporal change in divergence and rate of decrease of cloud top minimum temperature (top) for the Neosho storm.

Figure 4-6 shows the divergence and temperature change as a function of time for the Neosho storm. Near the times of the tornadoes, cloud top divergences were small, ($0.1 - 1.0 \times 10^{-3} s^{-1}$) and fairly large scatter existed. The storm top had apparently reached its minimum temperature also. The above points to the need for a bispectral or even multispectral method of observing severe storms. A microwave radiometer, with proper polarization, would be able to remotely sense the precipitation size particles below the anvil (Weinman and Guetter, 1977). Combined with visible channel radiances to detect overshoots and IR channel radiances for temperature, a nearly complete description of a storm from satellite sensors could be inferred.

4.4.3 Cloud no. 1

The growth rates of this hail producing storm are displayed in Figure 4-7. Though initially not as steep as those of the Wewoka storm, normalized rates of growth remain greater than 3×10^{-3} s^{-1} for several hours after the inception of the cloud. First reports of hail at 2325 GMT occurred during phases of growth as large as 5×10^{-3} s^{-1}. Of particular interest are the merging of three isotherms at 2325 with the anvil of the Wewoka storm. Scofield and Oliver (1977) and Purdom (1976b) discuss the importance of convective element mergers to the enhancement of convective rainfall and thunderstorm maintenance respectively.

4.5 Comparison with Non-Severe Storms

Most of the precipitating clouds examined in this study became severe at some point in their lifetime. There were, however, several clouds that formed at or near the times of those that did become severe. In Figure 4-2, clouds lettered A through E were all non-severe, with severity determined by reports published in Storm Data. Growth rates

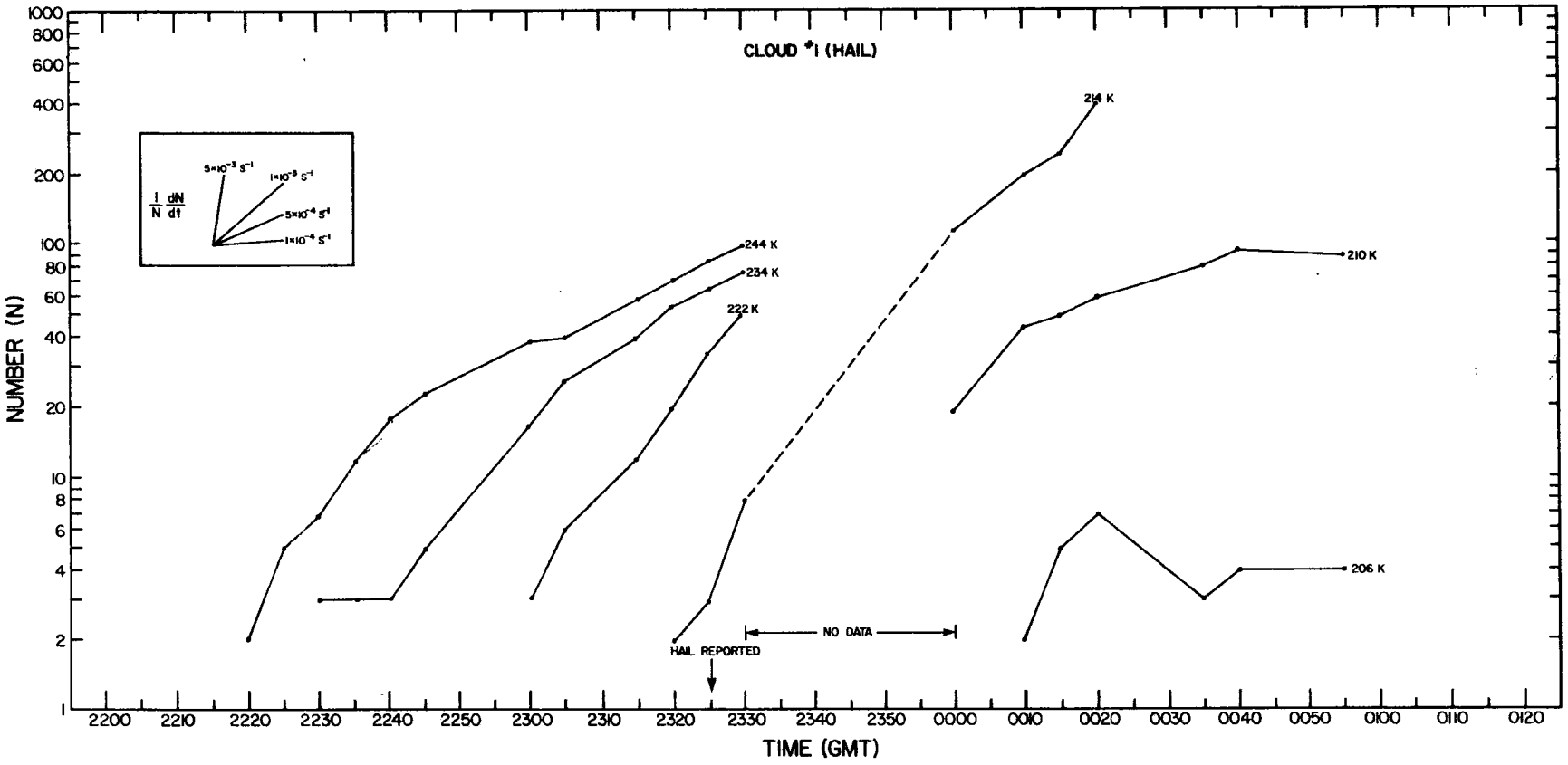

Figure 4-7 Thunderstorm growth rate diagram for cloud #1, a hail producer.

for three non-severe storms are presented in Figure 4-8. Differences between this figure and those for the severe storms are fairly obvious. First, the minimum blackbody temperature (T_{BB}) used to define these clouds had to be increased from 244 K (-29°C) to 256 K (-17°C). This is probably an underestimate of the true temperature due to non-unity emissivities at cloud edges with correspondingly "warmer" T_{BB}. A further problem might be one found by Negri et al. (1976). They found that the IR sensor did not correctly respond to clouds of small horizontal extent. The satellite has a rotation period of 0.6 s and only views the earth for five percent of that time. One scan is composed of 3822 IR pixels and thus the sensor will only "see" a cloud of 30 km width (7 pixels) for 5×10^{-5} s. This is approximately the response time (55 μsec) of the IR sensor and thus the correct response to the cold cloud radiance is not realized for clouds of small horizontal extent.

Several other apparent differences exist between severe and non-severe growth rates. In Figure 4-8, the duration of the clouds, as well as the number of pixels defining the clouds, are much less than those of the severe storms. Growth rates rarely exceed 1×10^{-3} s^{-1}, and in fact one element (Cloud D) had a negative rate of growth. Real time monitoring of growth rates on a frequent (5-15 minute) basis could identify clouds of probable severe potential early in their lifetime.

Monitoring of minimum blackbody temperature (T_{BB}) as well as growth rates can also provide an insight into storm severity. Figure 4-9 is a representation of minimum T_{BB} with time for two severe and two non-severe storms. The severe storms exhibited a much greater decrease in minimum T_{BB} than did the neighboring clouds. Minimum temperatures reached were 10-15°C colder for the severe storms. As was mentioned

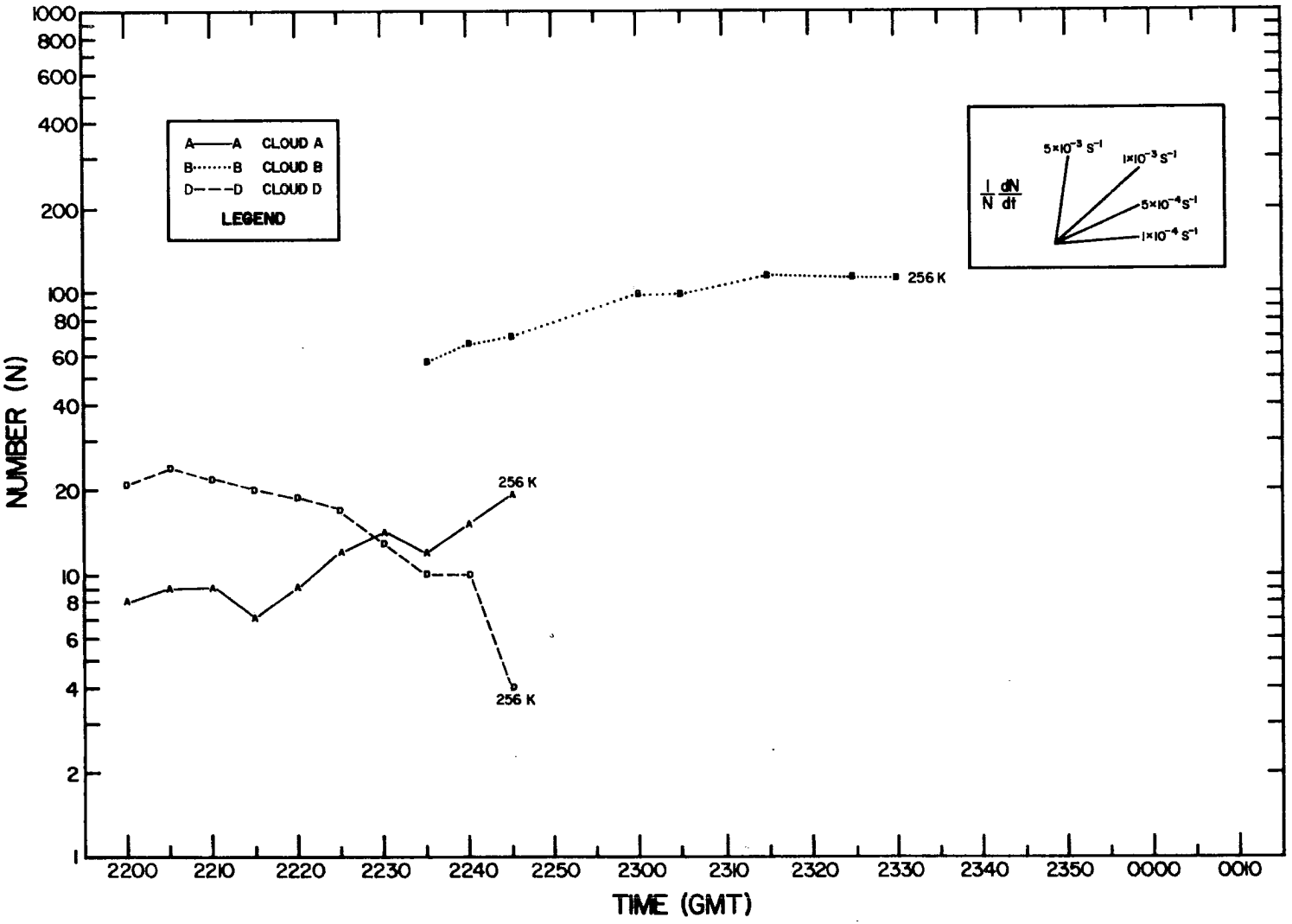

Figure 4-8 Thunderstorm growth rate diagram for several non-severe storms.

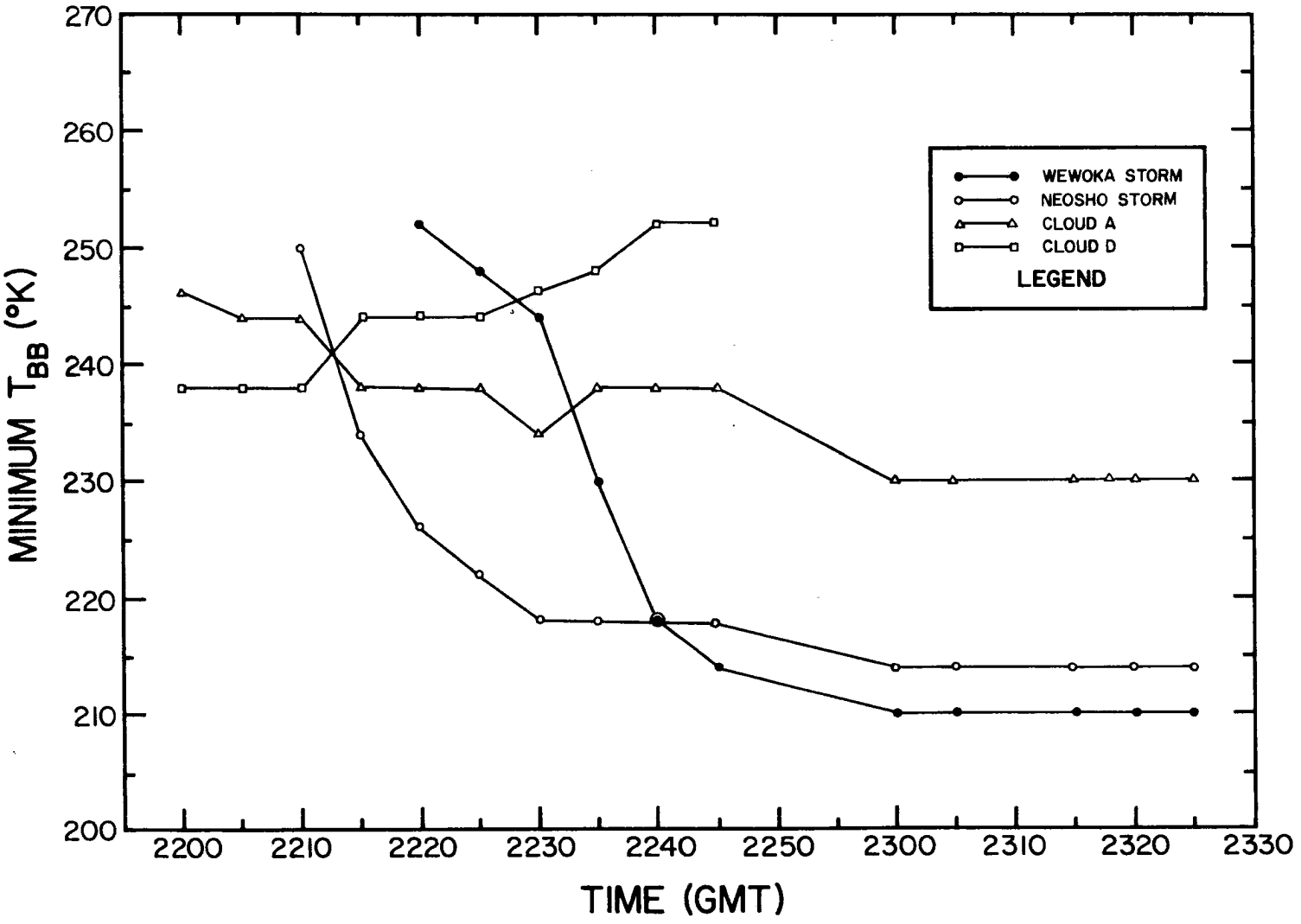

Figure 4-9 Temporal variation of minimum blackbody temperature (T_{BB}) for two severe and two non-severe storms.

previously, the time of occurrence of the severe event cannot be inferred from these temperature patterns.

4.6 Results for All Storms

On the basis of the above parameters a graphical summary of all clouds can be constructed which relates the severity of a storm to several key parameters. Adler and Fenn (1977) have done this for several storms that took place on 6 May 1975. Their results are reproduced in Figure 4-10. The graph shows the relation among cold area rates of growth, cloud top relative temperature, and the occurrence of severe weather. The quantity $(T_C - T_{MIN})$ is the cloud top relative temperature, where T_C is the minimum temperature achieved during the lifetime of a cloud element, and T_{MIN} is the minimum temperature of the coldest element during the entire lifetime of the cloud system. For a cloud that grows as cold or colder than the other clouds in the area, $(T_C - T_{MIN})$ will be zero. The values of $\frac{1}{N} dN/dt$ represent the maximum values, irrespective of temperature, for the very early stages of cloud growth. Their results show good agreement between normalized rates of growth greater than $3 \times 10^{-3} s^{-1}$ and storm severity, and also between low values of cloud top relative temperature and storm severity. This type of representation is fine for an after-the-fact analysis, but it cannot be used in real-time decision making because the minimum temperatures T_C and T_{MIN} are not known until <u>after</u> the occurrence (or non-occurrence) of severe weather. Thus, the technique was modified in this study for use as a real-time forecasting aid; only data for the first half hour of cloud lifetimes were used. This would provide an operationally significant time interval for decision making and dissemination of information. Results are presented in Figure 4-11.

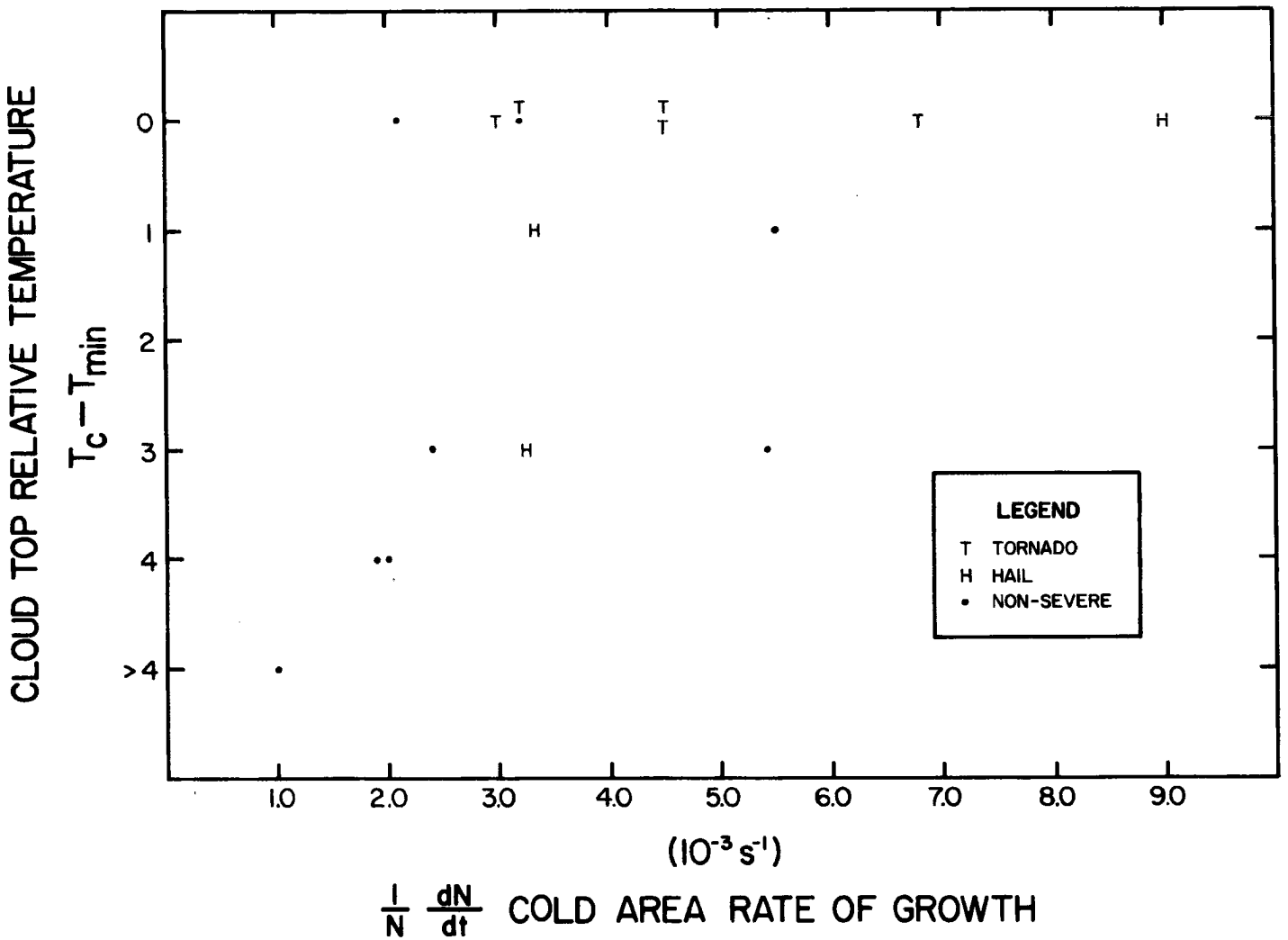

Figure 4-10 Relation of cold area rate of growth to cloud top relative temperature and the occurrence of severe weather (from Adler and Fenn, 1977).

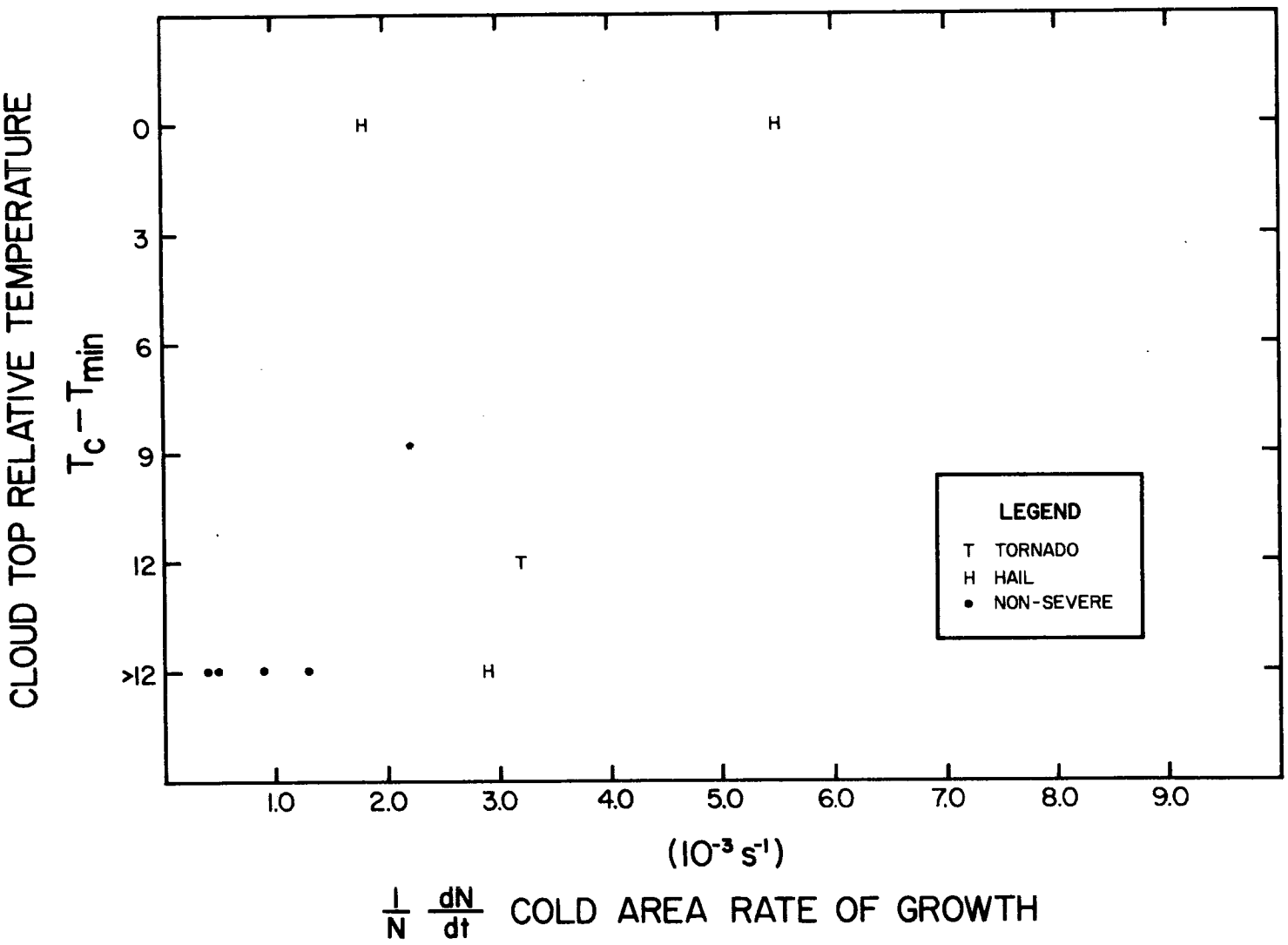

Figure 4-11 Results from this study using only the first 30 minutes of cloud lifetime.

The quantities (T_C-T_{MIN}) and $\frac{1}{N}\,dN/dt$ are still defined in the manner of Adler and Fenn, but are indicative of the very early stages of convective development. All non-severe storms had initial growth rates less than $1.3 \times 10^{-3} s^{-1}$, with correspondingly warmer minimum temperatures than the severe storms. For severe storms, normalized growth rates of $2.0 \times 10^{-3} s^{-1}$ or greater were found. It should be noted that sample size is very limited, and the need for a larger statistical sample from more case studies is needed. Despite this, it appears as though the early detection of severe weather producing clouds can be determined by frequent infrared monitoring by a geostationary satellite.

4.7 Summary of Infrared Growth Rates

It appears from this study that rapid interval SMS infrared digital data can be useful in the monitoring of severe local storms. Data of this temporal resolution (~5 minutes) are necessary for a "now-casting" capability for severe weather events. Several parameters may be calculated which are related to thunderstorm intensity and the occurrence of severe weather on the ground. In the early phase of cloud lifetime (first 30 minutes) criteria for a severe-non-severe decision should include:

1. the normalized rate of growth (or cloud-top divergence), $\frac{1}{N}\,dN/dt$. Maximum values greater than or equal to 2×10^{-3} were indicative of subsequent severe weather.

2. relative cloud-top temperature (T_C-T_{MIN}). Cloud elements 10-12°C colder than neighboring clouds are suspect as potential severe storms.

3. rate of change of minimum temperature. Cloud elements with decreases of 1.5°C/min in their early stages were found to have become severe.

4. duration and size. Non-severe cloud elements were found to be of smaller area and of shorter duration than severe elements. Larger and longer-lived clouds were of greater severe potential.

Predicting the time of initial hail or tornado occurrence was realized with a lesser degree of success. Reports of large hail occurred after several consecutive periods of rapid growth ($1 - 5 \times 10^{-3} s^{-1}$). However, the most destructive storm, the Neosho tornado, provided no discernable signatures in growth rate or temperature pattern. This is attributable to the late occurrence of the tornado below the cirrus anvil and to the inadequate infrared resolution of overshooting tops. Prior analysis by wind tracking, however, had indicated the high vorticity environment in which the Neosho storm developed. Results were in general agreement with those of Adler and Fenn, but were hindered by a lack of data prior to the tornado and by the small number of clouds used in the data base. No distinction was possible concerning the individual effects of wind shear and vertical velocity on the magnitude of the normalized rates of growth. It was assumed that the expansion of the cloud-top (due to generation of ice crystals) was due primarily to the intensity of the vertical motion.

Higher quality data will hopefully be available in the 1980's with the launch of StormSat, a 3-axis stabilized sounding and imaging system dedicated to mesoscale phenomena. Beyond that, the Synchronous Earth Observatory Satellite (SEOS) will provide improved visible and infrared sounding combined with microwave imaging and sounding.

5.0 RADAR-SATELLITE COMPARISON

5.1 Areal Comparisons

Radar data for the Wewoka hailstorm were available in the form of intensity contoured reflectivities (at zero degree elevation angle) from the WSR-57 radar at Oklahoma City (OKC). No radar data were available for the tornadic Neosho storm. The sequence of radar echoes between 2224 and 2329 GMT is shown in Figure 5-1. This interval represents the inception and growth phase of the Wewoka storm and includes the time span when two-inch and larger-sized hail was reported on the ground (2300-2315 GMT). In Figure 5-1, the location of all echoes is shown with respect to the fixed location of the OKC radar (denoted by the dark x's). The first echo developed south of the radar with subsequent echoes forming from southwest to northeast. The corresponding sequence of images as seen by the infrared (IR) sensor of the satellite is illustrated in Figure 5-2. The truly explosive growth of this storm can be seen as the tremendous increase of IR area in slightly over an hour. The horizontal scale and position of true north are indicated on the figure, but differ from those of Figure 5-1. When scale factors are taken into account, the entire radar echo area corresponds in areal extent to only a small portion of the infrared cloud area.

A more quantitative example of the radar echo growth of the Wewoka storm is portrayed in Figure 5-3, the radar echo area (km^2) as a function of time. The ordinate of the graph is logarithmic to facilitate a direct comparison with Figure 4-3, the infrared growth rate. Both the level 1 area (> 10 dbz) and the level 3 area (> 30 dbz) show initial periods of rapid growth followed by a slower growth after the occurrence of hail. Initial growth rates are of order 5×10^{-3} s^{-1}, virtually identical to those computed for the IR cloud area. The level 1 and

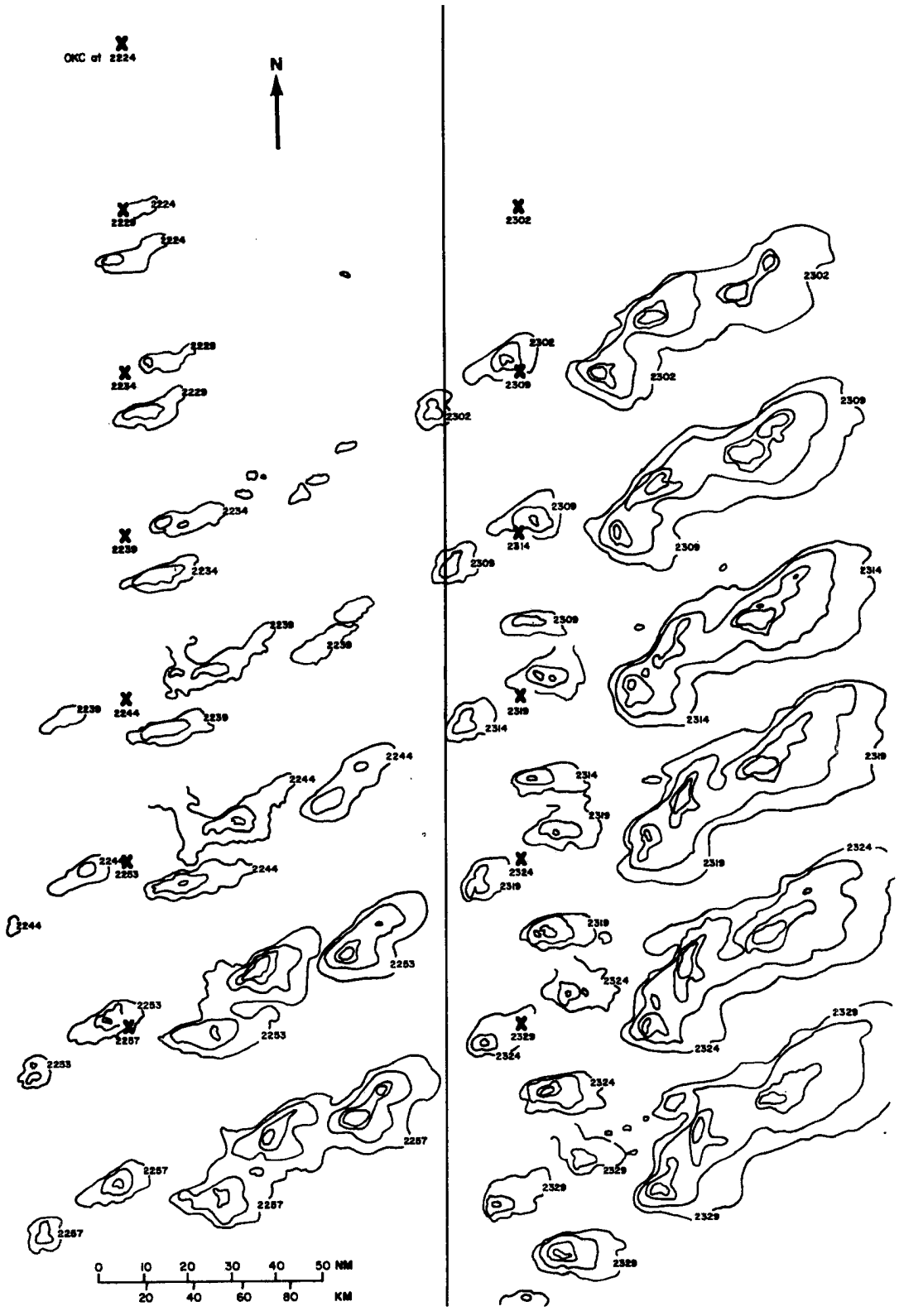

Figure 5-1 Intensity contoured radar reflectivities for the Wewoka storm.

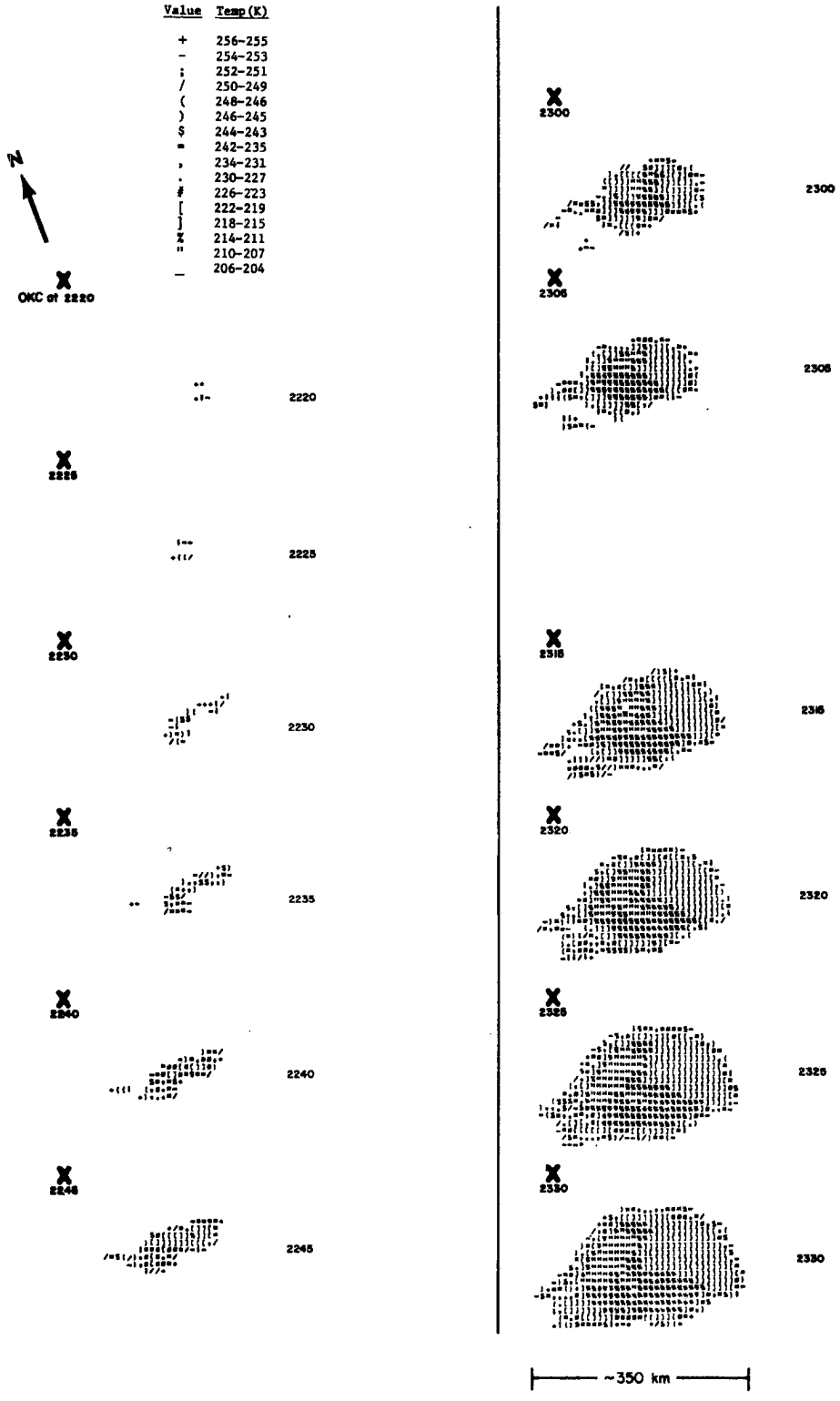

Figure 5-2 Character display of the infrared growth rate of the Wewoka storm.

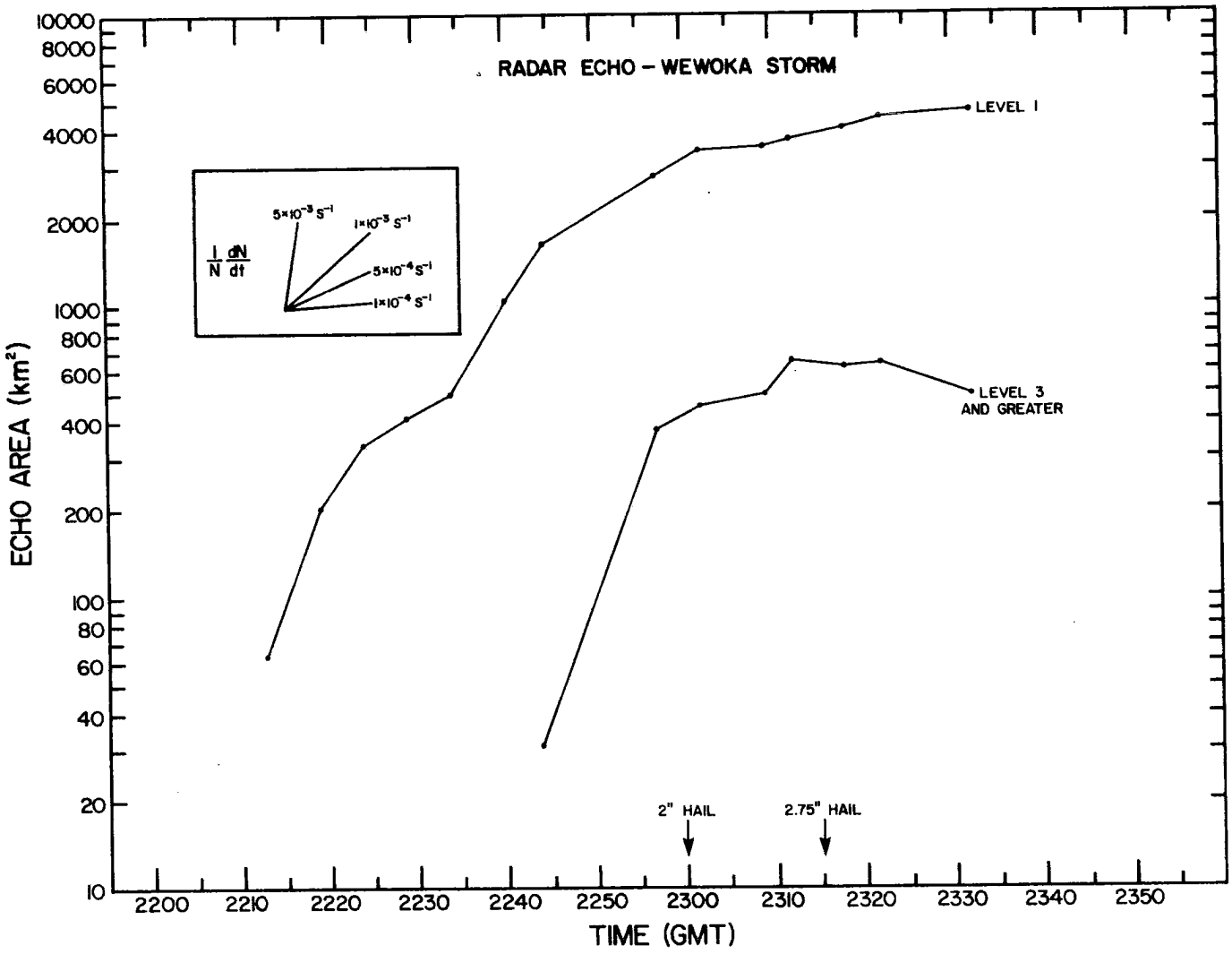

Figure 5-3 Radar echo growth rates for the Wewoka storm.

greater area was best related in actual value and in temporal variation to the area encompassed by the 244K (-29°C) isotherm on the satellite IR cloud. For a sample size of nine data points, the correlation coefficient of areas was 0.994. The level 3 and greater echo area, while well correlated with the temporal variation of the 210K (-63°C) isotherm, was of too small a magnitude to correspond specifically with any particular IR area. This is an indication that intense radar echoes of small horizontal extent cannot be detected as an IR signature underneath the expanding cirrus anvil. Small, intense echoes, as well as overshooting domes, have diameters of 10-12 km or cross-sectional areas of approximately 80 km^2. This is approximately the area of one IR data point (90 km^2) and thus the problem becomes one of resolution and sampling.

5.2 Storm Top Comparisons

The exact determination of cloud top height is of fundamental importance in weather forecasting and analysis. The vertical extent of a cloud is a measure of the intensity of its upward vertical motion. Thus, indirectly, vertical cloud extent is related to low-level convergance, subsequent release of latent heat, and eventually to the intensity of rainfall and to the degree of storm severity.

For the determination of cloud height from infrared radiances, we assume that a cloud emits radiation as a blackbody and that the cloud top temperature is the same as the environmental air temperature at that height. This was demonstrated by Pitts et al. (1975) from airborne radiometric measurements over severe storms. Particular problems can arise for small isolated clouds in a hot, dry environment due to radiometer response problems (Negri et al., 1976), but for large storms

extending to the tropopause the assumptions remain valid.

A direct comparison between radar and satellite heights was facilitated by the semi-isolated nature of the storms involved. National Weather Service (NWS) radar summaries were compared to nearly simultaneous (maximum difference of 9 minutes) blackbody temperature fields in an attempt to quantitatively assess cloud heights. Results are presented in Figure 5-4, a comparison of radar indicated cloud heights with heights derived from minimum IR temperatures and the Monett environmental sounding. The measurements were divided into three arbitrary time intervals, to examine the effect of the phase of cloud development on the radar-satellite height comparisons. Below the tropopause (~42,000 ft) there is fair agreement between heights determined by the two methods of sensing, with radar tops consistently higher than those derived by satellite measurements. For storms growing above the tropopause, determination of cloud tops from IR data alone was not possible.

The apparent ambiguity between the two methods of cloud top determination can be resolved if several factors are considered. First, the "inexactness" of reported heights on the NWS radar summaries may account for some of the scatter in Figure 5-4. These heights represent instantaneous values of the echo top as seen by one or more radars during a 20-minute period prior to the actual report. Given the magnitude of vertical velocity in a severe storm, echo tops can change in the vertical several thousand feet in just a few minutes. Smith and Reynolds (1976) have also found root mean differences of 2.53 km in studies of IR/radar height pairs.

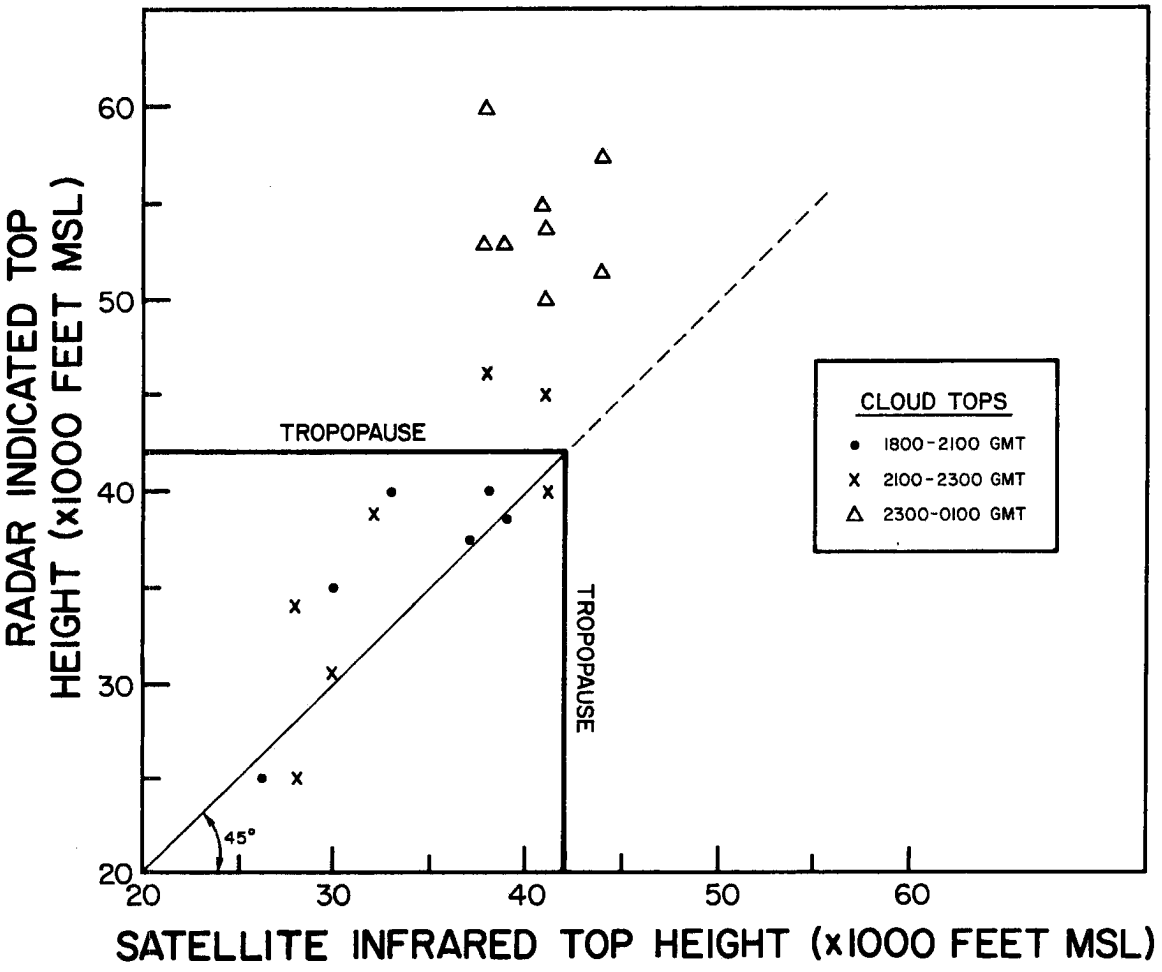

Figure 5-4 Comparison of radar and satellite indicated cloud top heights.

Infrared resolution and response may also impose limitations in inferring cloud heights. Overshooting domes of 10-12 km diameter will have cross sectional areas of approximately 80 km^2. The field of view (FOV) of the IR sensor at 35°N is approximately 90 km^2 so that an overshooting turret would have to be exactly centered in the FOV to return the correct radiometric response. Figure 5-5 shows a conceptual model illustrating this resolution problem. A cloud turret penetrating the tropopause will rapidly become much colder than its environment by cooling moist adiabatically. However, the small turrets are entraining environmental air whose temperature changes little with height because of the nearly isothermal lapse rate above the tropopause. The net effect is to smooth out the presence of the overshooting dome as viewed by the satellite IR sensor.

The finite response time of the IR sensor must also be considered when viewing small, isolated turrets above the anvil. We can relate the observed temperature (T_{meas}) to the effective blackbody temperature of the cloud (T_{eff}) by

$$T_{meas} = T_{eff} - \lambda \, dT/dN \qquad (5\text{-}1)$$

where λ is the lag coefficient (response) of the sensor and dT/dN is the temperature gradient along the direction of the scan.

A scan consists of 3822 pixels (1911 FOV's) completed while the sensor "sees" the earth for 5% of its rotation period (0.6 s). This allows each FOV to be viewed for 1.57×10^{-5} s. Since the response time of the sensor is 55×10^{-5} s, 3-4 FOV's are needed to realize a correct response at the satellite. Overshooting domes rarely provide this area in the infrared.

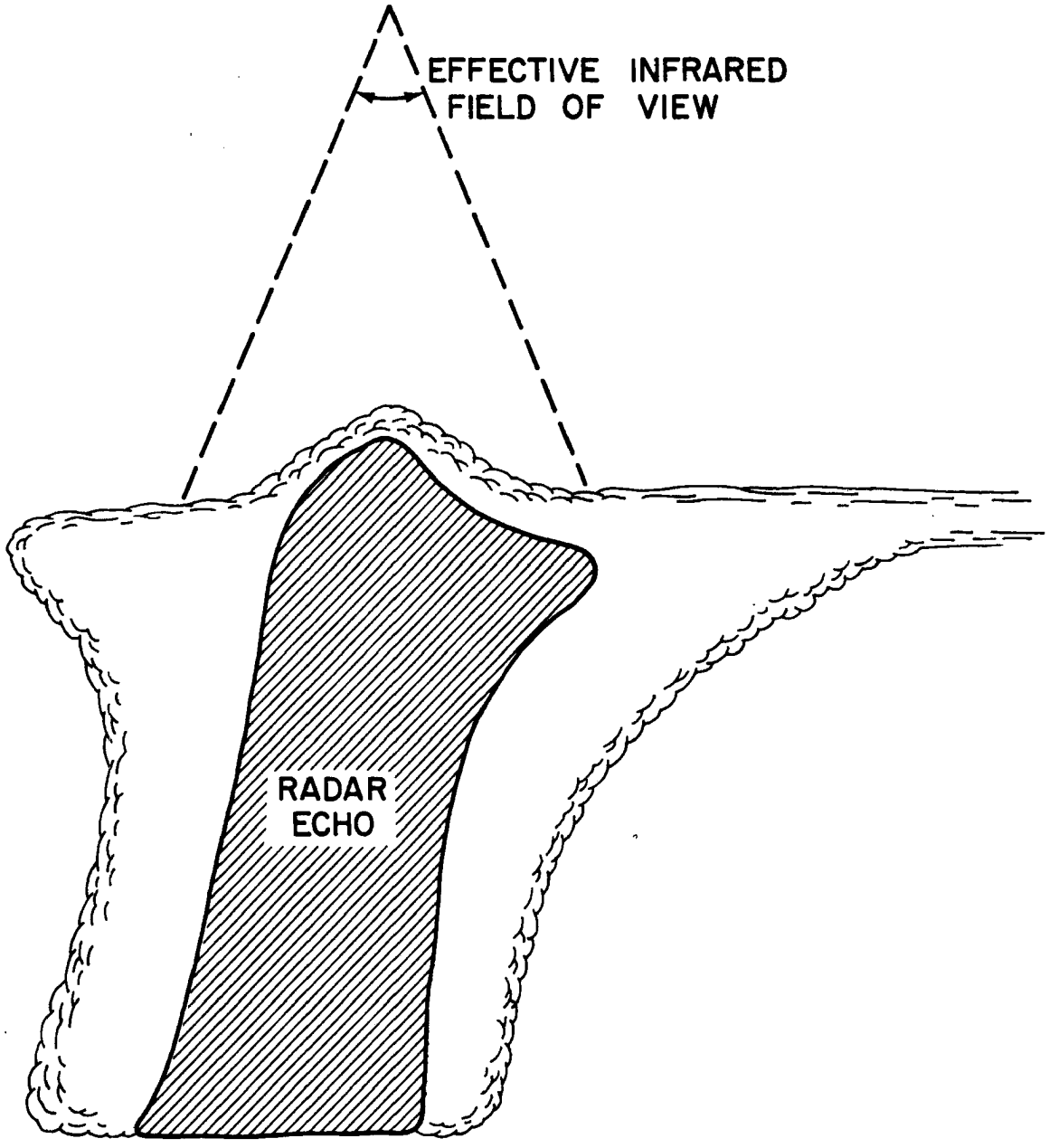

Figure 5-5 Conceptual model of satellite and radar viewed cloud area.

6.0 CONCLUSIONS

The approach taken in this study of severe local storms was essentially two-fold. The first technique utilized toward better prediction of severe storm genesis was the monitoring of the pre-storm environment through the use of satellite derived low-level wind fields. It was found that with the possible exception of not being exactly located in the vertical, the satellite wind fields provided a better representation of boundary layer flow then did corresponding surface winds. Wind fields coupled with surface mixing ratios as the representative moisture parameter allowed for the computation of moisture divergence in the pre-storm environment. Areas with moisture convergence values of $\sim 1.5 \times 10^{-3}$ g kg^{-1}s^{-1} or greater were found to be subsequent genesis areas of severe storms. Similar calculations using observed surface winds did not specify convective patterns as accurately. An equally representative moisture variable, total precipitable water, can be derived from vertical sounding of the (clear) atmosphere and combined with satellite wind fields. Thus, when a geosynchronous atmospheric sounder becomes available, moisture divergence fields may be determined solely from the vantage point of a satellite platform. As was demonstrated, simultaneous wind and moisture fields are desired if correlations between moisture convergence and severe storm genesis are to be considered valid.

The dynamic parameters of boundary layer "vorticity production" and relative vorticity also provided insight into the developmental nature of severe storms. When a region had both low-level convergence and large, positive relative vorticity, a local maximum in the rate of increase of vorticity is produced. Such maxima were spatially

correlated with regions of subsequent severe storm development. The contours of relative vorticity served to define the mesoscale nature of the dominant forcing mechanism (fronts, dry line, meso-low). The tornadic Neosho storm developed in an area of local maximum of relative vorticity. The sensitivity of the vorticity field to perturbations in the density and number of wind vectors illustrated an important limitation in tracking winds associated with real weather systems. This sensitivity would also seem to indicate the interdependence of the dynamic and moisture fields with the type of objective analysis scheme utilized. Future studies should include a structure function analysis of the wind fields to determine the "optimal" analysis scheme that should be used to minimize the noise and error.

A second technique of observation was applied after the initiation of a cloud element. In the early phase of cloud growth (first 30 minutes) the temporal change of cloud area was monitored. Infrared cloud radiances provided fields of equivalent blackbody temperature. Areal changes of representative isotherms are then proportional to cloud-top divergence, and thus indirectly to the vertical motion occurring beneath the cirrus anvil. Severe storms were found to have initial growth rates of 2×10^{-3} s^{-1} or greater, while non-severe storms grew out at a significantly slower rate. Neither the type of severe occurrence nor the time of occurrence on the ground could have been reliably predicted based on the cloud-top infrared signatures. The small sample size, however, limits the generalization of results. Relative cloud-top temperatures were another good indicator of storm severity, with clouds 10°C or colder than their neighbors generally becoming severe. Minimum temperature changes of 1.5°C min^{-1} or greater

were also indicative of storm severity. Some limitations in measuring growth rates in the infrared included the coarse resolution and finite response time of the sensor. The need for multispectral imaging of severe storms seems apparent. Such a multispectral technique might consist of cloud-top temperatures from infrared radiances, visible channel radiances to detect overshooting domes and a polarized microwave sensor to detect precipitation. The need for 5-minute interval coverage is also of importance because conventional 30-minute imagery cannot resolve the mesoscale and convective scale processes necessary to produce a short-term "point" forecast.

A detailed comparison of radar and satellite data was possible for the Wewoka hailstorm. Excellent correlation existed between temporal variation of total echo area and blackbody temperature contours. For intense echo area (> 30 dbz) no corresponding temperature contour could be identified. Using hourly NWS radar summaries, results indicated that for storms penetrating the tropopause, large scatter existed between radar-observed tops and those computed from blackbody temperatures and an environmental sounding. The problem is likely one of resolution; the infrared sensor cannot detect small, high-rising turrets nor small, intense echo areas beneath the cirrus anvil.

The utilization of a computer-linked, interactive video system to process and display digital imagery must also be an integral part of any "real-time" application of these techniques. The computer supplies the rapid processing and infinite patience necessary in displaying satellite data, while the satellite meteorologist can apply the known principles of atmospheric motion to produce as an integrated result a better severe local storm forecast. It is in this way that the real benefits of quantitative satellite measurements can be realized.

REFERENCES

Adler, R. F. and D. D. Fenn, 1976: Thunderstorm monitoring from a geosynchronous satellite. Preprint of Seventh Conf. on Aerospace and Aeronautical Meteorology and Symposium on Remote Sensing from Satellites, AMS, Melbourne, Florida, 307-311.

Adler, R. F. and D. D. Fenn, 1977: Satellite-based thunderstorm intensity parameters. Preprint of Tenth Conf. on Severe Local Storms, AMS, Omaha, Nebraska, 8-15.

Arn, R. M., 1975: Anvil area and brightness characteristics as seen from geosynchronous satellites. Master's Thesis, Colorado State University, Fort Collins, Colorado, 88 p.

Auvine, B. and C. E. Anderson, 1972: The use of cumulonimbus anvil growth data for inferences about the circulation in thunderstorms and severe local storms. Tellus, 24, 300-311.

Billingsley, J. B., 1976: Interactive image processing for meteorological applications at NASA/GSFC. Preprint of Seventh Conf. on Aerospace and Aeronautical Meteorology and Symposium on Remote Sensing from Satellites, AMS, Melbourne, Florida, 268-275.

Doswell, C. A., 1976: Subsynoptic scale dynamics as revealed by the use of filtered surface data. NOAA Tech. Mem. ERL NSSL-79, 40 p.

Endlich, R. M. and R. L. Mancuso, 1968: Objective analysis of environmental conditions associated with severe thunderstorms and tornadoes. Mon. Wea. Rev., 96, 342-350.

Fritsch, J. M., 1971: Objective analysis of a two-dimensional data field by the cubic spline technique. Mon. Wea. Rev., 99, 379-386.

Fujita, T. T., 1973: Proposed mechanism of tornado formation from rotating thunderstorm. Preprint of Eighth Conf. on Severe Local Storms, AMS, Denver, Colorado, 191-196.

Fujita, T. T., E. W. Pearl and W. E. Shenk, 1975: Satellite tracked cumulus velocities. J. Appl. Meteor., 32, 407-413.

Griffith, C. G., W. L. Woodley, S. Browner, J. Terjeiro, M. Maier, D. W. Martin, J. Stout, and D. N. Sikdar, 1976: Rainfall estimation from geosynchronous satellite imagery during daylight hours. NOAA Tech. Rep. ERL 356-WMPO 7, 106 p.

Hasler, A. F., W. E. Shenk, and W. C. Skillman, 1976: Wind estimates from cloud motions: phase 1 of an in situ aircraft verification experiment. J. Appl. Meteor., 15, 10-15.

Hillger, D. W. and T. H. Vonder Haar, 1976: Mesoscale temperature and moisture fields from satellite infrared soundings. Atmospheric Science Paper No. 249, Colorado State University, Fort Collins, Colorado, 66 p.

Hillger, D. W. and T. H. Vonder Haar, 1977: Deriving mesoscale temperature and moisture information from satellite radiance measurements over the United States. J. Appl. Meteor., 16, 715-726.

Holton, J. R., 1972: An introduction to dynamic meteorology. Academic Press, New York and London, 319 p.

Houghton, D. D. and T. A. Wilson, 1975: Mesoscale wind fields for a severe storm situation determined from SMS cloud observations. Preprint of Ninth Conf. on Severe Local Storms, AMS, Norman, Oklahoma, 187-192.

Hudson, H. R., 1971: On the relationship between moisture convergence and convective cloud formation. J. Appl. Meteor., 10, 755-762.

Maddox, R. A., A. J. Negri, and T. H. Vonder Haar, 1977: Analysis of satellite derived winds for 24 April 1975. Preprint of Tenth Conf. of Severe Local Storms, AMS, Omaha, Nebraska, 54-60.

Negri, A. J., D. W. Reynolds, and R. A. Maddox, 1976: Measurements of cumulonimbus clouds using quantitative satellite and radar data. Preprint of Seventh Conf. on Aerospace and Aeronautical Meteorology and Remote Sensing from Satellites, AMS, Melbourne, Florida, 119-124.

Negri, A. J., D. W. Hillger, and T. H. Vonder Haar, 1977: Moisture convergence from a combined mesoscale moisture analysis and wind field for 24 April 1975. Preprint of Tenth Conf. on Severe Local Storms, AMS, Omaha, Nebraska, 48-53.

Oliver, V. J. and R. A. Scofield, 1976: Estimation of rainfall from satellite imagery. Preprint of Sixth Conf. on Weather Forecasting and Analysis, AMS, Albany, New York, 242-245.

Ostby, F. P., 1975: An application of severe storm forecast techniques to the outbreak of June 8, 1974. Preprint of Ninth Conf. on Severe Local Storms, Norman, Oklahoma, 7-12.

Peslen, C. A., 1977: A satellite interpretation of the dynamics of a severe local storm area using 5-minute interval SMS data. Preprint of Tenth Conf. on Severe Local Storms, AMS, Omaha, Nebraska, 1-7.

Pitts, D. E., W. K. Reeser, and M. A. Mendlowitz, 1975: Equivalent blackbody temperature of the top of a severe storm. J. Appl. Meteor., 14, 609-618.

Purdom, J. F. W., 1976a: Tornadic thunderstorms and GOES satellite imagery. Paper presented at Ninth Conf. on Severe Local Storms, AMS, Norman, Oklahoma, 5 p.

Purdom, J. F. W., 1976b: Some uses of high resolution GOES imagery in the mesoscale forecasting of convective and its behavior. Preprint of Sixth Conf. on Weather Forecasting and Analysis, AMS, Albany, New York, 260-267.

Ray, P. S., C. E. Hane, R. P. Davies-Jones, and R. L. Alberty, 1976: Tornado-parent storm relationship deduced from a dual-Doppler radar analysis. Geophysical Research Letters, 3, 721-723.

Sasaki, Y. K., 1973: Mechanism of squall line formation as suggested by variational analysis of hourly surface observations. Preprint of Eighth Conf. on Severe Local Storms, AMS, Denver, Colorado, 300-307.

Sasaki, Y. K., 1975: Variational analysis and dynamics of severe local storms. Final report submitted to NOAA, U.S. Department of Commerce, Boulder, Colorado.

Schaefer, J. T., 1973: On the computation of the surface divergence field. J. Appl. Meteor., 12, 546-547.

Scofield, R. A. and V. J. Oliver, 1977: A scheme for estimating convective rainfall from satellite imagery. NOAA Tech. Mem., NESS 86, 47 p.

Smith, E. A. and D. W. Reynolds, 1976: Comparison of cloud top height determinations from three independent sources: Satellite IR measurements, satellite viewed cloud shadows, radar. COSPAR Ninteenth Plenary Meeting, Philadelphia, PA, 17 pp.

Suchman, D. and D. W. Martin, 1976: Wind sets from SMS images: An assessment of quality for GATE. J. Appl. Meteor., 15, 1265-1278.

Tegtmeier, S. A., 1974: The role of the surface, sub-synoptic, low pressure system in severe weather forecasting. Master's Thesis, University of Oklahoma, Norman, Oklahoma, 66 p.

Viezee, W., S. M. Serebreny, and R. L. Mancuso, 1972: A sample computation of kinematic properties from cloud motion vectors. J. Appl. Meteor., 11, 731-741.

Weinman, J. A. and P. J. Guetter, 1977: Determination of rainfall distribution from microwave radiation measured by the Nimbus-6 ESMR. J. Appl. Meteor., 16, 437-442.

Whitney, L. F., 1977: Relationship of the sub-tropical jet stream to severe local storms. Mon. Wea. Rev., 105, 398-412.

Wilson, G. S., 1976: Large-scale vertical motion calculations in the AVE IV experiment. Geophysical Research Letters, 3, 735-738.

ACKNOWLEDGMENTS

The author would like to express his deep appreciation to his advisor, Dr. Thomas H. Vonder Haar, for his advice and encouragement during the course of this study. The input and guidance provided by Dr. Peter C. Sinclair and by Dr. Philip D. Kearney is also acknowledged. For their critical review of this manuscript, as well as for their constant academic and moral support, the author is especially grateful to Robert Maddox and David Reynolds.

Other invaluable assistance included computer programming aid by Ms. Charline Polifka, drafting by Ms. Janella Owen, photograph reduction by Duane Barnhart, and expert typing by Mrs. Debbie Bonser. Kelly Hill, of NASA Marshall Space Flight Center, provided the AVE-IV upper air data. This research was supported by the National Aeronautics and Space Administration under Grant NSG-5011 and by the National Science Foundation under Grant ATM 76-21307.

APPENDIX A

ALL DIGITAL VIDEO IMAGING SYSTEM FOR ATMOSPHERIC RESEARCH

APPENDIX A

ALL DIGITAL VIDEO IMAGING SYSTEM FOR ATMOSPHERIC RESEARCH

The All Digital Video Imaging System for Atmospheric Research (ADVISAR) is a sophisticated blend of hardware and software components designed to let the user interact subjectively with his data set. It is particularly suited to the satellite meteorologist who often has a temporal sequence of images, each of which may have as many as 10^8 "words" or discrete pieces of information. The overall system is described in terms of its five component subsystems:

1. Computer hardware and peripherals
2. Video display hardware and control
3. Digitizing hardware and control
4. System executive software
5. Applications software

A pictorial view of the ADVISAR is shown in Figure A-1. Individual hardware components are lettered and are listed in Table A-1. Accessible data storage consists of eight 512 x 512 rapid refresh video memories. So for instance, eight consecutive images can be fashioned into a temporal loop and displayed under computer or manual control. Dynamic enhancement tables allow the user to select a range of data values and to adjust the input/output "lookup" according to his specific needs. An electronic cursor allows the user access to every element in the 512 x 512 array. Modular programming permits a relatively naive user to write his own meteorological parameter extraction technique (i.e., wind tracking, growth rates, bispectral imaging) which can then be run in conjunction with existing applications software. Such a system is limited solely by the imagination of its users.

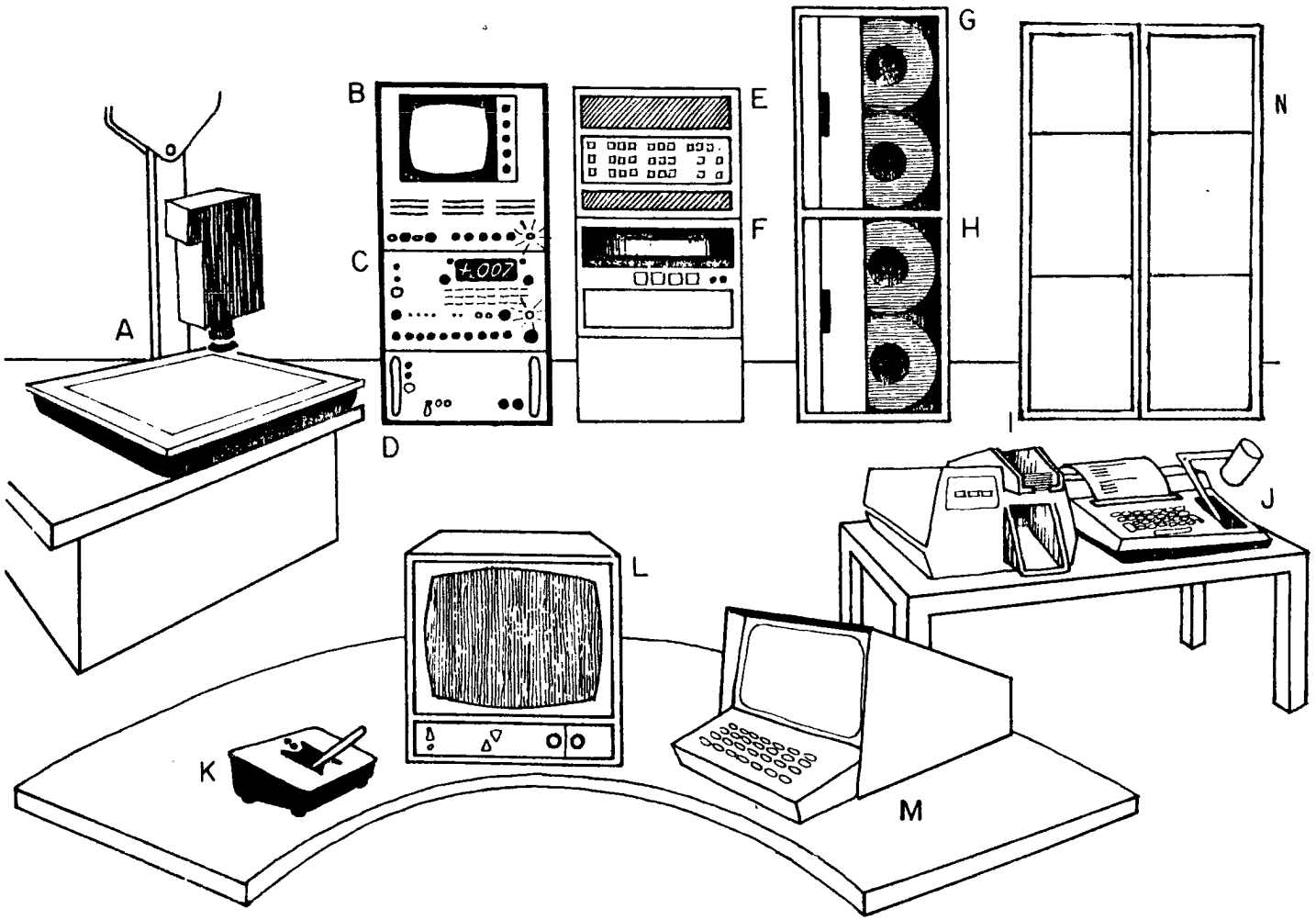

Figure A-1 All Digital Video Imaging System for Atmospheric Research (ADVISAR).

Table A-1. All Digital Video Imaging System for Atmospheric Research (ADVISAR)

A	DIGITIZING SUB-SYSTEM
B	108 CONTROLLER AND B/W MONITOR
C	DATA COLOR EDGE ENHANCER
D	SCAN CONVERTER
E	HP 2100-A COMPUTER
F	DIGITAL DISK
G	9 TRACK DRIVE
H	7 TRACK DRIVE
I	CARD READER
J	SYSTEM TELEPRINTER AND KEYBOARD
K	JOYSTICK
L	COLOR DISPLAY MONITOR
M	OPERATOR CRT AND KEYBOARD
N	SOLID STATE RAPID VIDEO REFRESH MEMORIES

APPENDIX B

GLOSSARY OF TERMS

APPENDIX B

GLOSSARY OF TERMS*

conditional instability--the state of a column of air in the atmosphere when its lapse rate of temperature is less than the dry-adiabatic lapse rate but greater than the saturation-adiabatic lapse rate

convection--atmospheric motions that are predominantly vertical, resulting in vertical transport and mixing of atmospheric properties.

difluence--the rate at which adjacent flow is diverging along an axis oriented normal to the flow at the point in question

entrainment--the mixing of environmental air into a pre-existing organized air current so that the environmental air becomes part of the current.

frontogenesis--an increase in the horizontal gradient of an air mass property, and the development of the accompanying features of the wind field that typify a front.

infrared radiation--electromagnetic radiation lying in the wavelength interval from about 0.8 microns to an indefinite upper boundary usually set at 100 microns (0.01 cm)

lapse rate--the decrease of an atmospheric variable with height, the variable being temperature, unless otherwise specified

level of free convection (LFC)--the level at which a parcel of air lifted dry-adiabatically until saturated and saturation-adiabatically thereafter would first become warmer than its surroundings in a conditional unstable atmosphere

lifted condensation level (LCL)--the level at which a parcel of moist air lifted dry-adiabatically would become saturated

lifted index--a measure of the potential instability computed by lifting the mean moisture in the lower 3,000 feet of the atmosphere moist-adiabatically to 500 millibars and subtracting the temperature at this point from the reported 500 millibar free-air temperature

mesoscale meteorology--this field is concerned with the detection and analysis of the state of the atmosphere as it exists between meteorological stations

mixing ratio--the dimensionless ratio of the mass of water vapor to the mass of dry air.

*Definitions from Glossary of Meteorology, edited by Ralph E. Huschke, American Meteorological Society, Boston, MA (1959) 638 p.

precipitable water--the total atmospheric water vapor contained in a vertical column of unit cross-sectional area extending between any two specified levels

shortwave--with regard to atmospheric circulation, a progressive wave in the horizontal pattern of air motion with dimensions of 1000 to 2500 km

Showalter index--a measure of the local static stability of the atmosphere, expressed as a numerical index

synoptic scale--the study and analysis of weather information on a scale of 1000 to 2500 km

thickness--the vertical depth, measured in geometric or geopotential units, of a layer in the atmosphere bounded by surfaces of constant pressure

tropopause--the boundary between the troposphere and stratosphere, usually characterized by an abrupt change of lapse rate

vapor pressure--the partial pressure exerted by molecules of water vapor in the atmosphere

vorticity--a vector measure of local rotation in a fluid flow, defined mathematically as the curl of the velocity vector.

BIBLIOGRAPHIC DATA SHEET	1. Report No. CSU-ATSP-278	2.	3. Recipient's Accession No.
4. Title and Subtitle Satellite Observations of the Onset and Growth of Severe Local Storms			5. Report Date December, 1977 6.
7. Author(s) Andrew J. Negri (P.I. Thomas H. Vonder Haar)			8. Performing Organization Rept. No. 278
9. Performing Organization Name and Address Atmospheric Science Department Colorado State University Fort Collins, Colorado 80523			10. Project/Task/Work Unit No. 11. Contract/Grant No. NASA Grant NSG-5011 & NSF Grant ATM 76-21307
12. Sponsoring Organization Name and Address National Aeronautics and Space Administration Goddard Space Flight Center Greenbelt, Maryland 20770		National Science Foundation Washington, D.C. 20550	13. Type of Report & Period Covered 14.
15. Supplementary Notes			

16. Abstracts On 24 April 1975, numerous severe storms developed in an area extending from southwest Oklahoma to eastern Tennessee during the afternoon and evening hours. Significant severe weather reports included 2.75 in. hail at Wewoka, Oklahoma and a destructive, killer tornado at Neosho, Missouri. An unusually comprehensive data set was available on this day that included: 5-minute interval SMS visible and infrared radiances from 1800 to 0200 GMT; intensity contoured radar reflectivities; special upper-air analyses from NASA's Atmospheric Variability Experiment; and low-level wind fields from satellite inferred cumulus velocities.

The mesoscale nature of the forcing and evolution of these storms is investigated, with emphasis on techniques to aid in the early detection of such severe events. In the pre-storm environment (t-4 to t-2 hours), the satellite wind fields were combined with moisture parameters to derive horizontal moisture flux information. Low level moisture convergence of $1.5 \times 10^{-3} g\ kg^{-1} s^{-1}$ or greater was indicative of regions of subsequent severe storm genesis. Dynamic parameters such as boundary layer vorticity production and relative vorticity were also useful prognosticators of subsequent severe activity.

In the first 30 minutes of cloud lifetime, infrared (IR) cloud growth rates of $2 \times 10^{-3} s^{-1}$ or greater accurately indentified potential severe storms. Little success was realized in forecasting the exact time of the severe event on the ground. A comparison of IR determined cloud tops with radar observed tops illustrated particular problems in inferring cloud height for storms penetrating the tropopause. The need for rapid-time interval satellite coverage is stressed, as is the need for a computer-linked video system to process and interpret data.

17. Key Words and Document Analysis.

Severe Storms
Satellites
Thunderstorms
Cloud Tracking
SMS

17c. COSATI Field/Group

18. Availability Statement	19. Security Class (This Report) UNCLASSIFIED	21. No. of Pages 89
	20. Security Class (This Page UNCLASSIFIED	22. Price